Chapter 9

9. Case Studies for the Optimum Design of Chain Pillars in Deep Longwall Workings

9.1 General

Currently, deep Longwall mining in India is practised only at Moonidih Colliery in Jharia Coalfield and Adriyala Longwall Project in Godavari Valley Coalfield. This chapter outlines the findings of the studies to evaluate the optimum size of chain pillars for both these mines (Table 9.1). Three case studies pertaining to seam I of Adriyala mine, and one case study pertaining to each of XVIII, XVI Top, and XV Top seams at Moonidih Colliery have been covered for this purpose.

Table 9.1 The geo-mining details of the case studies

S. No.	Mine	Seam	Adjoining Panels	Extraction height (m)	Cover depth (m)	Field Pillar width (m)	Face length (m)	RMR of the coal seam
1.	Adriyala	I	P1-P2	3.5	465	50	250	43
2.			P2-P3		519	63		
3.			P3-P4		567	69		
4.	Moonidih	XVIII	A4-A5	2.5	392	45	95	49
5.		XVI Top	D12-D13	2.6	580	50	150	56.6
6.		XV Top	T3-T4	3.65	865	60	250	37.4

All these case studies involve a single row configuration of the chain pillars. However, Moonidih Colliery faces a more significant challenge in meeting the ventilation requirements at the deep working faces owing to Degree III gassiness and high strata temperature (BCCL, 2022). It is extremely challenhing to provide efficient ventilation in highly mechanised workings involving long headings for controlling the temperature and relative humidity of

ventilating mine air. Although a high-capacity main mechanical ventilator ventilates the mine, the challenge persists in ventilation at the working face. The management is looking for more efficient methods to deal with the challenge, especially given the operational depth reaching around 900m in the XV Seam. To this end, the design of the double row chain pillar has been examined for the XV Top Seam working.

9.2 Site and Geo-mining Details

9.2.1 Adriyala Longwall Project

The Adriyala Longwall Project is situated in the Ramagundem coal belt in the Pedapalli district of Telangana, India. The areal extent of the project is 4.63 sq. km, while the length along the strike direction is 2.6 km. The site has a latitude of 18^0 39'03" to $18^0$40'34" in the North and a longitude of $79^0$34'28" to $79^0$35'55" in the East. The four coal seams I, II, III, and IV out of the seven seams IA, I, II, IIIB, IIA, III, and IV are envisaged for extraction. The life of the project is 35 years, and its planned production capacity is 2.81 MPTA. The total geological reserve is 110 Mt up to the depth of 650 m. Figure 9.1 shows the project location and geological map of the coalfield.

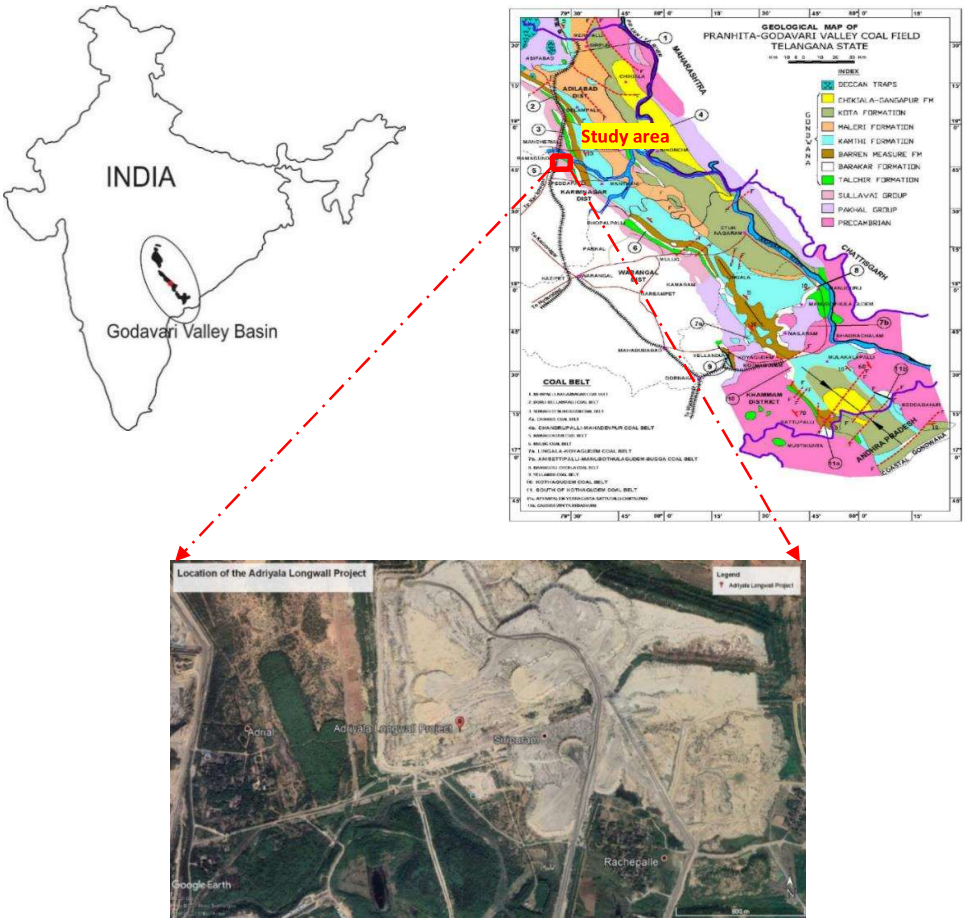

Figure 9.1 Geological map of Godavari Valley Coalfield (modified after scclmines.com, accessed on 21 Dec. 2021) and location of the Adriyala longwall project

A total of 16 longwall panels (4 panels in each seam - I, II, III, and IV) are planned to be extracted. The four panels in Seam I are to be extracted with the face length and extraction height of 250 m and 3.5 m, respectively. The average thickness and gradient of the seam are 5.7m and 1 in 6, respectively. The cover depth of the panels ranges from 362-720 m. The size of the chain pillars between the panels P1-P2, P2-P3, and P3-P4 is 50 m, 63 m and 69 m, respectively (Fig. 9.2). The depth of cover for the chain pillars between the panels P1-P2, P2-P3 and P3-P4 are 465 m, 519 m, and 567 m, respectively. The gate roads are 5.2 m wide and 3.5 m high.

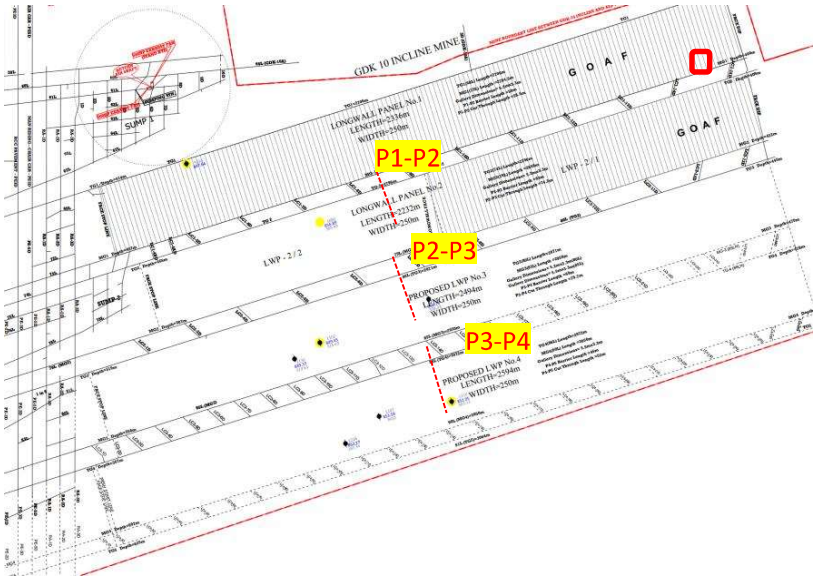

Figure 9.2 Layout of the mine plan of the Adriyala Longwall Project (ALP) site

Table 9.2 The characteristics of the roof strata and their properties in Panel P1

Strata	Rock type	Thickness (m)	RQD (%)	Density (kg/m^3)	σ_c (MPa)	σ_t (MPa)	Young's Modulus (GPa)
Overburden	Cgsst	410.00	50	2046	16.77	1.96	5.20
Main roof	Mgsst, Cg-vcgsst, Cgsst, shalycoal	29.40	84	1964	13.22	1.25	2.86
Immediate roof	Cg-vcgsst, Mgsst	23.20	89	2030	13.86	1.07	4.28
Coal roof	Coal, shalycoal	2.40	43	1870	27.58	2.30	2.00
Coal seam	Coal	3.50	40	1400	27.58	2.30	2.00

The study of strata characteristics in the mine showed that the shale and mudstone are present near the coal seams, and the inter-burden between the adjoining seams is formed of sandstone (Table 9.2). The compressive strength of the overlying rock strata varies from 7.1 to 27.6 MPa, whereas the tensile strength ranges from 0.6 - 2.3 MPa. The RQD of the overlying rock beds

varies between 43 and 93%. The strata are primarily comprised of coarse to very coarse-grained sandstone. The RMR value of the coal seam is 43. Hence, the coal seam is at the boundary of the 'Poor' and 'Fair' categories in the classification table.

The observations of the Telltale extensometers in the travelling roadway (Tailgate of the second panel, TG2) showed that the cumulative convergence increased monotonically with the time and location of the face in the first panel (Srikanth et al., 2019) (Figure 9.3). The convergence ceased to increase when the face was 300 – 500 m past the instrument location. The convergence in the TG2 after its development varied from 15-25 mm, which increased to 80-110 mm upon extraction of the first panel.

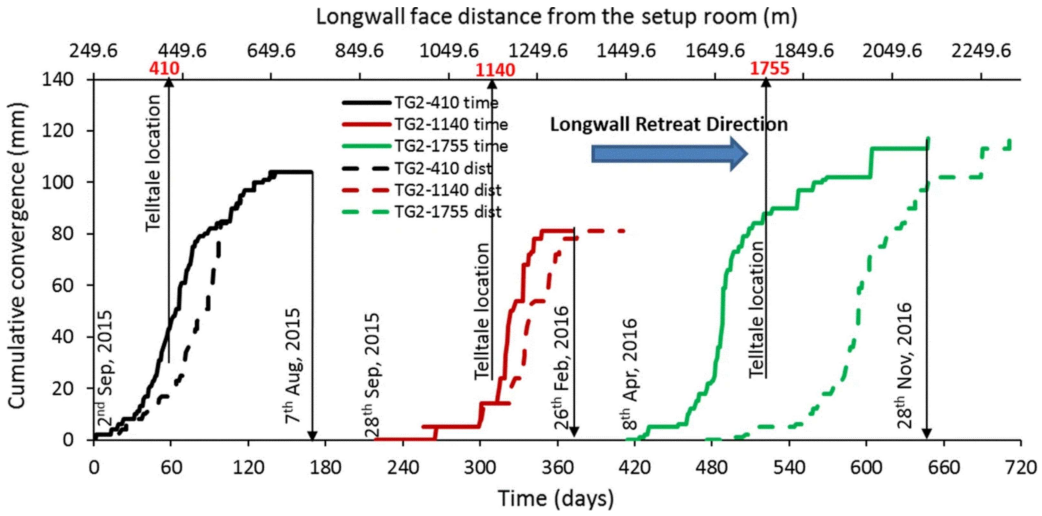

Figure 9.3 Cumulative convergence in the tailgate (TG2) with time and the retreat of the face in the first panel (after Srikanth et al., 2019)

9.2.2 Moonidih Colliery

Moonidih Colliery is located in the central part of the Jharia Coalfield (Figure 9.4). It is situated between the latitude of 23^0 42' 47'' to 23^0 45' 42'' North and the longitude of 86^0 19' 21'' to 86^0 22' 26'' East. It is one of the largest underground coal mines in India, with a total geological

reserve of 1240.8 MT. It is the pioneer of Powered Support Longwall working (PSLW) in India, introduced in 1978. Six coal seams of thickness ranging from 0.33 to10.77 m have been identified in this mine up to the cover depth of 1200 m. With the depth of current workings ranging from 450-650m, it is also the deepest underground coal mine in India (BCCL, 2022).

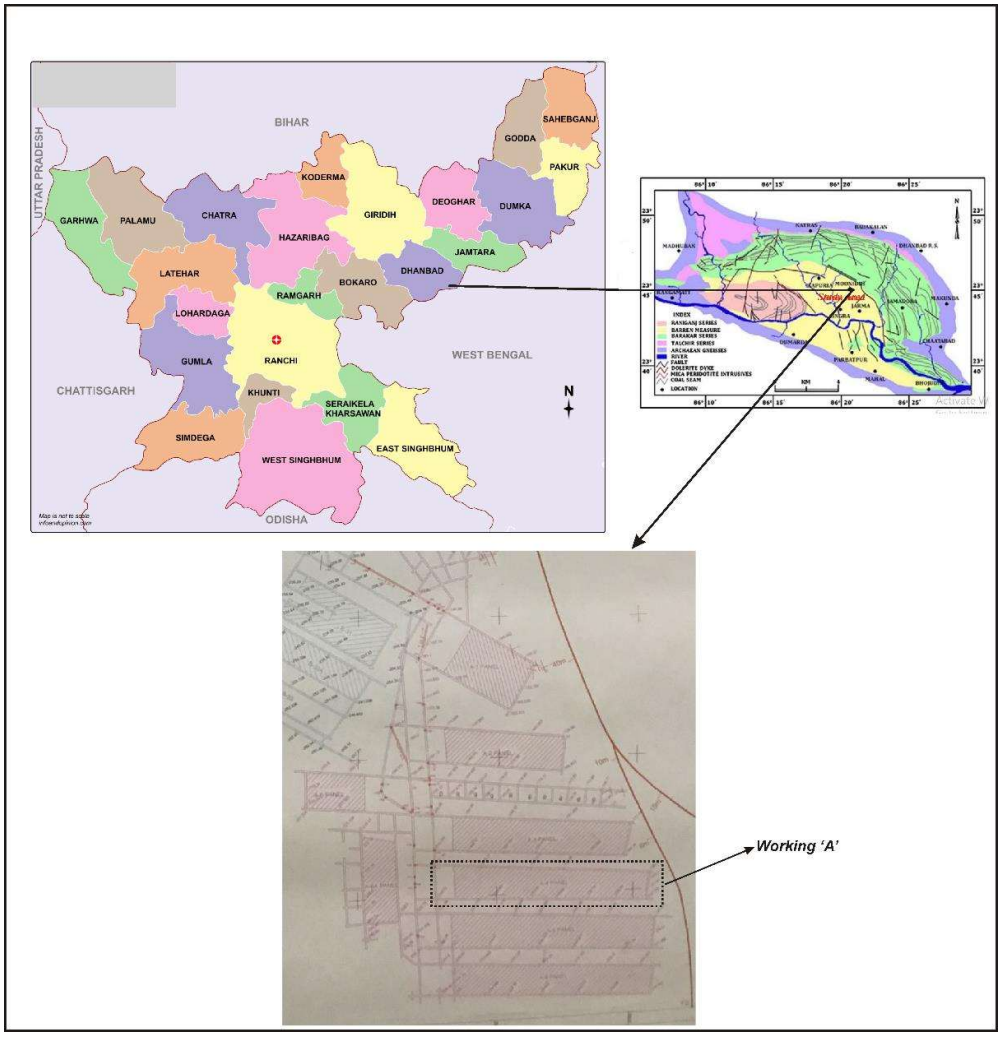

Figure 9.4 Geological map of Jharia Coalfield and location of the Moonidih mine

9.2.2.1 The XVIII Seam working

The study area in the XVIII Seam working pertains to the chain pillars between Panels A4 and A5 (Fig. 9.4). The size of the intervening chain pillar in the mine was 45 m (c-c). The longwall

panels A4, A5, A6, and A8, were extracted with 95 m face length. The average height of extraction and cover depth of these workings were 2.5 m and 392 m, respectively. The rock characteristics of the strata overlying the longwall panels, as revealed from the lithological details of borehole MND 3 drilled over panel A4, are given in Table 9.3. The immediate roof was comprised of shaly coal and intercalation, whereas the main roof was composed of medium to coarse-grained sandstone, coal, shaly coal, and intercalation. The compressive and tensile strengths of the strata varied from 10.2 - 44.7 MPa and 0.2 - 4.5 MPa, respectively, whereas the RQD of the strata ranged from 40 – 73%. The RMR of the coal seam was 49.

Table 9.3 Rock characteristics of the strata overlying A4 panel at Moonidih mine

trata	Rock type	Thickness (m)	RQD (%)	Density (kg/m^3)	σ_c (MPa)	σ_t (MPa)	Young's Modulus (GPa)
Overburden	Mgsst, intercalation, Fgsst	370.35	64	2144	41.48	3.24	12.77
Main roof2	Mgsst, intercalation, cgsst, coal, shaly coal	10.17	62	2003	30.77	2.77	6.04
Main roof1	Intercalation coal, shalycoal	5.34	57	1935	37.55	3.58	6.21
Immediate roof	Intercalation, shalycoal	5.64	47	1879	34.62	3.22	5.07
Coal	Coal	3.65	40	1406	10.20	0.22	2.00

The field observation of convergence in the tailgate of the second panel shows that the roof-to-floor convergence after the development and the extraction of the first panel ranged from 10-30 mm and 40-70mm, respectively.

9.2.2.2 The XVI Top Seam Working

A total of 10 longwall panels (D8, D9, D10, D11, D12, D13, D15, D11A D16, and D17) were planned for extraction in the XVI Top seam of Moonidih Colliery. Out of these, eight panels have been mined successfully without any strata control problems with the chain pillar width of 50 m. The average depth of the coal seam varies from 406 m in Panel-D17 to 650 m in Panel-D15. There is no worked-out coal seam either above or below the coal seam in this patch of the mining area. The coal seam is Degree III gassy. The immediate roof is primarily comprised of shale, whereas the floor consists of sandstone. The width of the chain pillars between the panels is 50m (c-c), whereas the gate road width is 4.5 m. The average gradient of the seam is 1 in 7. The average thickness of the coal seam varies from 2.08 m in D-17 panel to 2.8 m in D-15 panel. All the panels have a face length of 150 m except Panel D-16 wherein the face length is 136 m. The study area pertains to the chain pillar between Panels D12 and Panel-D13 (Figure 9.5A). The cover depth at this site is 580 m.

The characteristics of strata overlying XVI Top seam in the mine were studied using the lithology of strata as revealed from boreholes MNN 3 and MNN5 (at the easternmost end and western part of the Panel-D13, respectively). Table 9.4 shows the lithology and the physico-mechanical properties of the strata. The 14.4 m thick main roof is formed of medium to coarse-grained sandstone. Most rock beds are formed of 'laminated formations of shale and sandstone', Intercalation and medium-grained sandstone with shale bands. Rock beds of shale and coarse-grained sandstone are also present. The % of sandstone content in the strata varies from 52 to 70. The formation of rock beds is almost similar in most of the panels. The record of convergence in the tailgate of the second panel showed that the roof-to-floor convergence after the development and the extraction of the first panel ranged from 10 – 35 mm and 35 – 85 mm, respectively.

Table 9.4 Physico-mechanical properties of strata in XVI Top seam Working at Moonidih Colliery

Strata	Rock type	Thickness (m)	RQD (%)	Density (kg/m^3)	σ_c (MPa)	σ_t (MPa)	Young's Modulus (GPa)
Overburden	Mgsst, Fgsst, Cgsst, Shalysst	554.00	81	2144	32.54	2.54	12.77
Loading roof	Cgsst, Fgsst, Shalysst	6.27	70	2797	75.69	11.63	8.44
Main roof	Mgsst, Fgsst, Cgsst, Shalysst	14.41	81	3019	60.05	9.08	7.73
Immediate roof	Mgsst, Shale, Shalysst	4.86	53	3240	59.96	10.60	6.75
Coal	Coal	2.60	40	1330	5.40	0.55	2.00

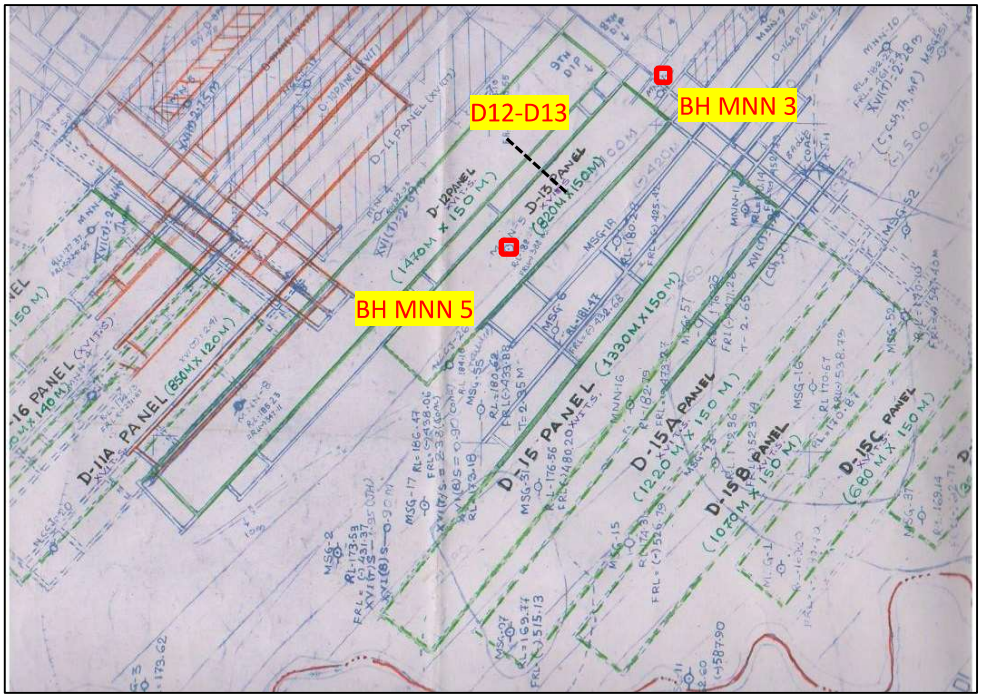

Figure 9.5 Part plan showing the location of longwall panels in XVI Top seam

9.2.2.3 The XV Seam Working

The XV seam is geologically encountered in two sections at Moonidih mine: XV Top and XV Bottom. The average thickness of the XV Top seam is 3.65 m, while the XV Bottom seam is 5.15 m thick. A number of longwall panels are proposed to be worked with a face length of 250 m in each section following non-simultaneous extraction in descending order. The longwall panels (Figure 9.6) are proposed to be worked using a single row of rectangular chain pillars of 60m width (c-c). The proposed width and height of gate roads are 5.7 m × 3.6 m. The parting between the two sections is formed of shaly sandstone, and its thickness varies from 3 to 15 m. The cover depth in the Top Section workings varies from 620 to 865 m.

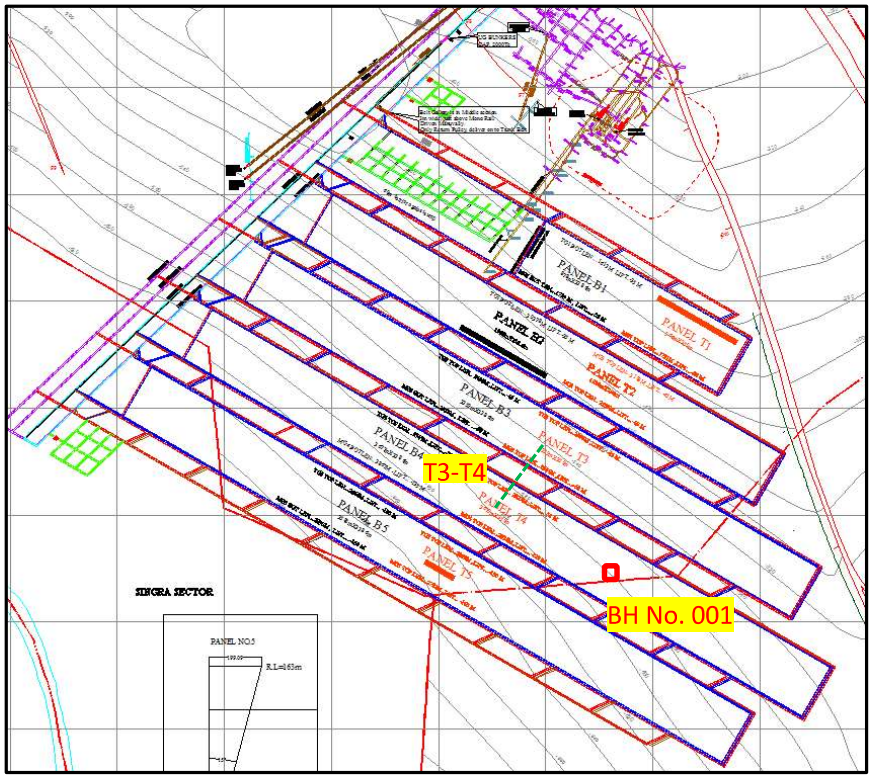

Figure 9.6 Part plan showing the location of proposed longwall panels in XV Top and Bottom coal seams

The characteristics of strata overlying XV Top seam have been referred from the section of borehole BH No. 001 (Fig. 9.6). The thickness weighted average of density, compressive strength, tensile strength and RQD of 93 m thick strata over the coal seam have been used as their representative properties. The physico-mechanical properties of coal and strata were determined from laboratory testing of rocks. The final dataset obtained for this study is given in Table 9.5.

Table 9.5 Physico-mechanical properties of XV Top and Bottom Coal Seams and its Parting at Moonidih Colliery

Strata	Rock type	Thickness (m)	RQD (%)	Density (kg/m^3)	σ_c (MPa)	σ_t (MPa)	Young's Modulus (GPa)
Overburden	Micaceous Fgmgsst, shale, Mgsst	865	84	2350	43.25	12.64	13.39
XV Top	Coal	3.6	40	1443	6.38	1.18	2.0
Parting	Fgmgsst, Cgsst	3.0	81	2498	47.5	9.94	14.73
XV Bottom	Coal	3.60	40	1443	6.38	1.18	2.00

The compressive strength of the overlying rock strata varies from 10.97-69.94 MPa, whereas tensile strength ranges from 2.28-10.71 MPa. The RQD of the overburden varies between 44 and 100. The RMR of the coal seam is 37.4.

9.3 Determination of the Optimum Pillar Size

The calibrated numerical models developed in previous chapters were utilised to evaluate the factor of safety of the chain pillars under study. The rock mass properties (Table 9.6) of the longwall workings under study were estimated from the laboratory-measured intact rock strength data using the approach suggested by Singh and Singh (2009).

Table 9.6 Rock mass properties for the numerical model of Longwall Workings at Adriyala Longwall Project and Moonidih Colliery

	Thickness (m)	Density kg/m^3	Shear Mod. (GPa)	Bulk Mod. (GPa)	Tensile strength (MPa)	Cohesion (MPa)
P1-P2, P2-P3, P3-P4 Panels, ALP mine						
Overburden	395.00	2046	2.80	4.67	0.49	0.98
Main Roof	29.40	1976	1.14	1.91	0.52	1.29
Immediate Roof	23.20	2026	1.71	2.85	0.49	1.96
Coal Roof	2.40	1592	0.80	1.33	0.47	1.80
Coal	3.50	1592	0.80	1.33	0.47	1.80
Floor	200	2046	2.08	3.47	0.49	0.98
A4-A5 Panels, XVIII seam, Moonidih Colliery						
Overburden	337.40	2144	5.11	8.51	1.03	3.08
Main Roof2	10.17	2003	2.42	4.03	0.86	2.22
Main Roof1	5.34	1935	2.48	4.14	1.03	2.52
Immediate Roof	5.64	1879	2.03	3.38	0.76	1.90
Coal Roof	1.10	1406	0.80	1.33	0.04	0.65
Coal	2.55	1406	0.80	1.33	0.04	0.65
Floor	200	1935	2.48	4.14	1.03	2.52
D12-D13 Panels, XVI Top seam, Moonidih mine						
Overburden	336.26	2144	5.11	8.51	1.03	3.08
Loading Roof	6.27	2797	3.38	5.63	4.07	6.19
Main Roof	14.41	3019	3.09	5.15	3.68	5.68
Immediate Roof	4.86	3240	2.70	4.50	2.81	3.71
Coal	2.60	1330	0.80	1.33	0.11	0.34
Floor	200	2144	3.09	5.15	3.68	5.68
T3-T4 Panels, XV Top seam, Moonidih mine						
Overburden	865	2350	5.36	8.93	5.32	4.25
XV Top	3.60	1443	0.80	1.33	0.10	0.38
Parting	3.00	2498	5.89	9.82	4.02	4.49
XV Bottom	3.60	1443	0.80	1.33	0.10	0.38
Floor	200	2523	5.36	8.93	5.32	4.25

The material properties of the Double-yield model for the goaf material in the Caved zone were estimated using the standard approach proposed in Section 6.4, Chapter 6. The angle of internal friction and the dilation angle for the goaf material was taken as 20° and 10°, respectively, while the Poisson's ratio of 0.2 was assumed. The initial modulus of the goaf material was

estimated by calibrating the model to match the subsidence profile of Adriyala Longwall workings (Figure 6.7, Chapter 6), while the modulus for the rest of the workings was evaluated using Yavuz (2004) formula in the absence of any kind of subsidence at the surface because of the Non-Effective Width-to-Depth ratio in these workings. Table 9.7 presents the properties of the goaf material.

Table 9.7 Material properties of the Double yield model for Caved Goaf

Seam, Mine	Density (kg/m^3)	Bulk Modulus (GPa)	Shear Modulus (GPa)	Initial Modulus (E_0, MPa)
Seam-I, ALP	1976	1.81	1.36	23.4
XVIII, Moonidih	2017	3.89	2.92	26.4
XVI Top, Moonidih	2709	4.95	3.71	52.9
XV Top, Moonidih	2350	7.44	5.58	32.0

The strength and deformational properties of the Ubiquitous-joint model for the Fractured zone and the Transversely Isotropic model for the Continuous Deformation zone were estimated using the approach described in Sections 6.5-6.6, Chapter 6. The average Geological Strength Index (GSI) was taken as 30 to determine the rock mass modulus from the laboratory modulus. The ratio of modulus in the horizontal direction (E_1) to that in the vertical direction (E_3) was 1.72, while the shear modulus in the vertical direction (G_{13}) was 33MPa in the Transversely Isotropic model. The abutment angle was determined using the statistical model (Equation 7.3) developed in Chapter 7. The elastic moduli E_1 and E_3 and the abutment angle are shown in Table 9.8. The coal seam was assigned 'Elastic' model to estimate the factor of safety of the pillars using Equations 3.26-3.28 (Section 3.14, Chapter 3).

Table 9.8 Material properties of the Transversely Isotropic model and the Abutment angle

Seam/Mine	Pillar	E_1	E_3	Abutment angle (°)
	P1-P2			9.2
Seam-I, ALP	P2-P3	31.7	54.5	7.6
	P3-P4			6.6
XVIII, Moonidih	A4-A5	77.8	134	3
XVI Top, Moonidih	D12-D13	77.8	134	4
XV Top, Moonidih	T3-T4	81.6	140	11

Parametric studies for various widths of the chain pillars were conducted to determine the optimum size of the chain pillars. The pillar width was varied from 42-80 m for P1-P2, 45-65 m for P2-P3, and 49-69 m for P3-P4, while it was varied from 15-45 m for A4-A5 (XVIII seam), 25-50 m for D12-D13 (XVI seam), and 40-70 m for single-row and 30-50 m for double-row chain pillars between panels T3-T4 in XV seam of Moonidih mine. Further, the Machine Learning (ML) models developed in Chapter 8 were also utilised to evaluate the safety factor of the chain pillars for single and double-row configurations. Figures 9.7 (i-vi) show the comparative plot of the factor of safety with the changing width of the chain pillars in different cases. The outcomes of the ML models are in close agreement with the numerical model.

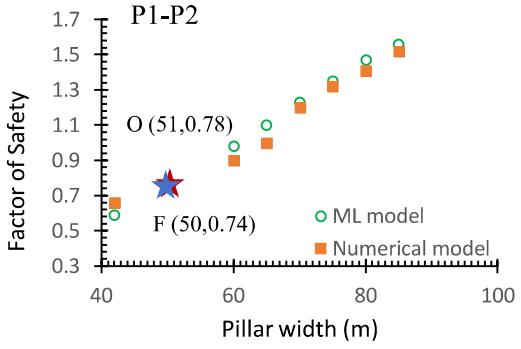

(i)

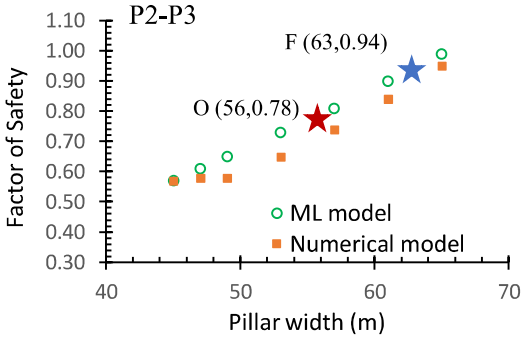

(ii)

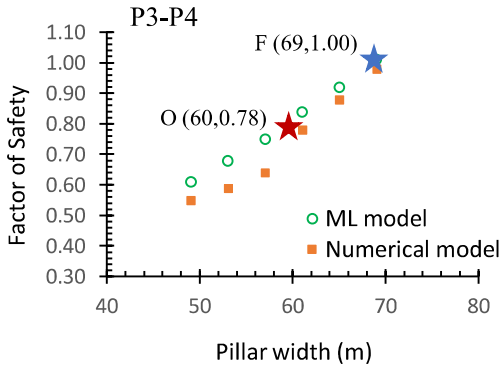

(iii)

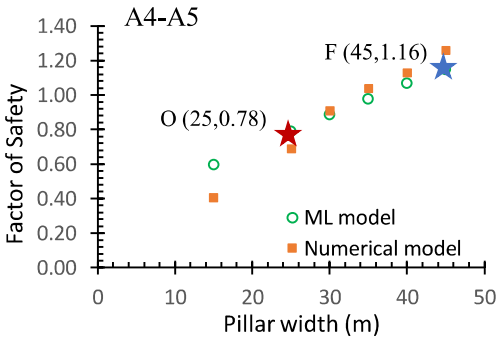

(iv)

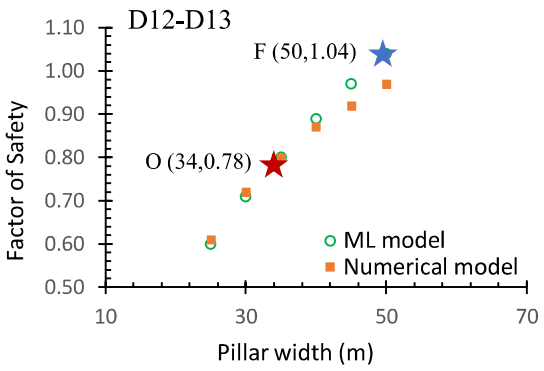

(v)

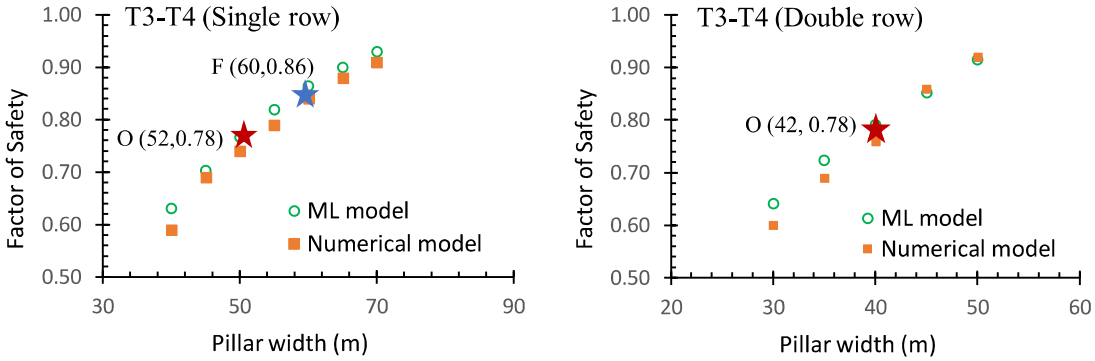

(vi-a) (vi-b)

Figure 9.7 Variation in the factor of safety of the chain pillars of different widths between (i) P1-P2, (ii) P2-P3, (iii) P3-P4, (iv) A4-A5, (v) D12-D13, (via) T3-T4 Single row, and (vib)T3-T4 double row. The blue and red star symbols depict the pillar width practised in the field and their optimum value estimated by the ML model

The design criterion developed in Chapter 5 was used to evaluate the optimum size pillar. As per the criterion, chain pillars should be designed for the safety factor of 0.78 to fail when both the adjoining panels have been extracted, thus completing the isolation requirement between the panels and producing a gradual and smooth subsidence profile at the surface. At this stage, the pillar is subjected to maximum loading during the entire loading cycle. Table 9.9 summarises the safety factor of the chain pillar implemented in the field and the corresponding optimum pillar width for the cases under study.

Table 9.9 Safety factor of chain pillars implemented in the field and their optimum width

Seam, Mine	Pillar	Field Pillar width (m)	FoS for field size pillar width	Optimum pillar width, m	Coal Conservation
Seam-I, ALP	P1-P2	50	0.74	51	-2.00
	P2-P3	63	0.94	56	11.11
	P3-P4	69	1.00	60	13.04
XVIII, Moonidih	A4-A5	45	1.16	25	44.44
XVI Top, Moonidih	D12-D13	50	1.04	34	32.00
XV Top, Moonidih	T3-T4	60	0.86	52	13.33

The FoS of the pillars between panels P1-P2, P2-P3, and P3-P4 at the Adriyala Project varies between 0.74 - 1.00. The chain pillar for panels P1-P2 was adequately designed, while the chain pillars for the other panels were overdesigned by 11-13%. The implementation of the optimal size pillars could help the mine in improved coal recovery by reducing the width of inter-panel chain pillars by 7- 9 m without any compromise on the stability of workings.

The chain pillars between the panels A4-A5 of 95 m face length in the coal seam XVIII were significantly overdesigned. These panels could have been worked with an optimal pillar width of 25 m in place of 45 m practised in the field. A similar result was noted for the Top Seam working, where the optimum width of the chain pillar was indicated as 34 m in place of 50 m as proposed by the mine. The chain pillars between the panels D12-D13 and T3-T4 could be reduced by 16 and 8 m, respectively. For the double row configuration of chain pillar T3-T4 in XV Top Seam, the optimum width of the pillar size was estimated as 42 m.

9.4 Elasto-Plastic Modelling Results

A numerical study was conducted with Mohr-Coulomb strain-softening (MCSS) model for the coal seam to develop an in-depth understanding of the pillar behaviour at different stages of loading. The post-peak softening parameters for the coal pillars were estimated using Equations 4.1-4.4 (Section 4.5, Chapter 4). The behaviour of the pillar was analysed in terms of stress redistribution, the extent of the failure, gate road convergence for one-sided goaf, and lateral confinement due to the interface effect.

9.4.1 Chain pillar between Panels P1-P2 in Adriyala Seam-I Working

When the gate roads or panels are excavated, the equilibrium states of in-situ stresses are destroyed. These stresses are redistributed to achieve the new equilibrium conditions. Consequently, a de-stressed zone develops in the roof of the excavated structure, and redirected stresses are concentrated into the solid coal of the pillars and the panel. The knowledge of these stresses is critically important for understanding the failure mechanism (Suchowerska et al., 2014). Figures 9.8 (a)-(d) show the profile of the vertical stress distribution for optimum pillar width of 50m along with the profiles for 60, 70, and 80m wide pillars. The last three widths were included for a comparative study wrt the optimum size pillars. Prior to excavation, the vertical stress of 9.7 MPa was uniformly distributed in the seam. The stress redistribution after the gate road excavations led to stress concentration up to 11.3 MPa in the ribs along the gate roads for different pillar widths. Two peaks were observed in the stress profile when the first panel was mined. The peak vertical stress in the pillar was 19.4, 17.9, 17.4, and 17.3 MPa for 50m, 60m, 70m, and 80m widths, respectively. For 70 and 80 m wide pillars, the peak stress was located at the goaf side pillar rib. The maximum stress recovery of 7.4 MPa (78.7% of the in-situ stress) was observed in the caved goaf at a distance of 57 m (0.12H) from the panel edge in all four cases.

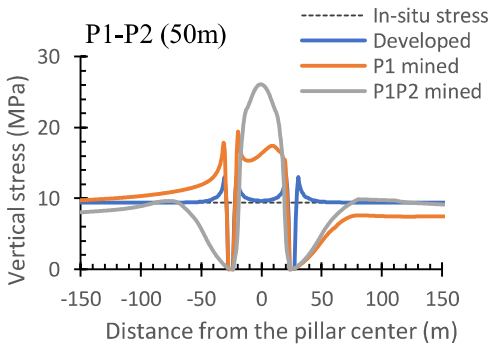

(a)

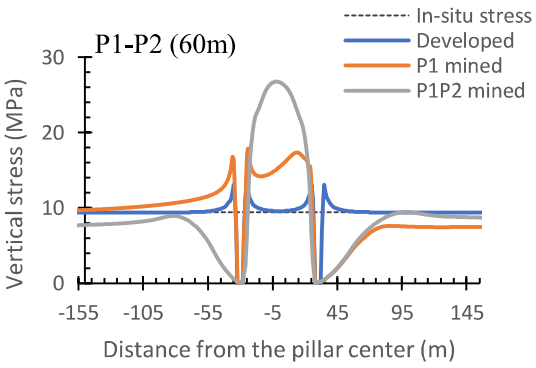

(b)

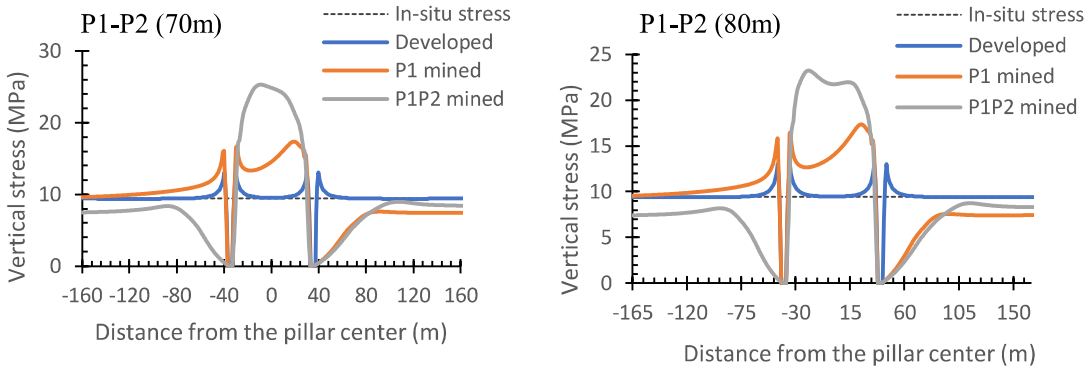

(c) (d)

Figure 9.8 Distribution of vertical stress in the chain pillars of (a) 50, (b) 60, (c) 70 and (d) 80 m width after the development of gate roads, mining of the first panel (P1 mined), and mining of both the adjoining panels (P1P2 mined)

When both the adjoining panels were mined, the stress profile witnessed a single peak for 50, 60, and 70 m wide pillars and a double peak for 80 m wide pillar. The peak vertical stress was 26.1, 26.7, 25.3, and 23.1 MPa for pillar widths of 50, 60, 70, and 80 m, respectively. The peak stress was concentrated at the centre of 50 m and 60 m wide pillars, whereas it was concentrated at the pillar rib towards the goaf of the second panel for 70 m and 80 m wide pillars. The maximum recovery of goaf stress in the first panel reached the in-situ value for pillar widths of 50 and 60 m, whereas it was about 90% of the in-situ stress for 70 and 80 m pillars. The maximum stress recovery in the second panel was approximately equal to the in-situ value for pillar widths of 50 and 60 m, whereas it was 80% of the in-situ stress for 70 and 80 m wide pillars.

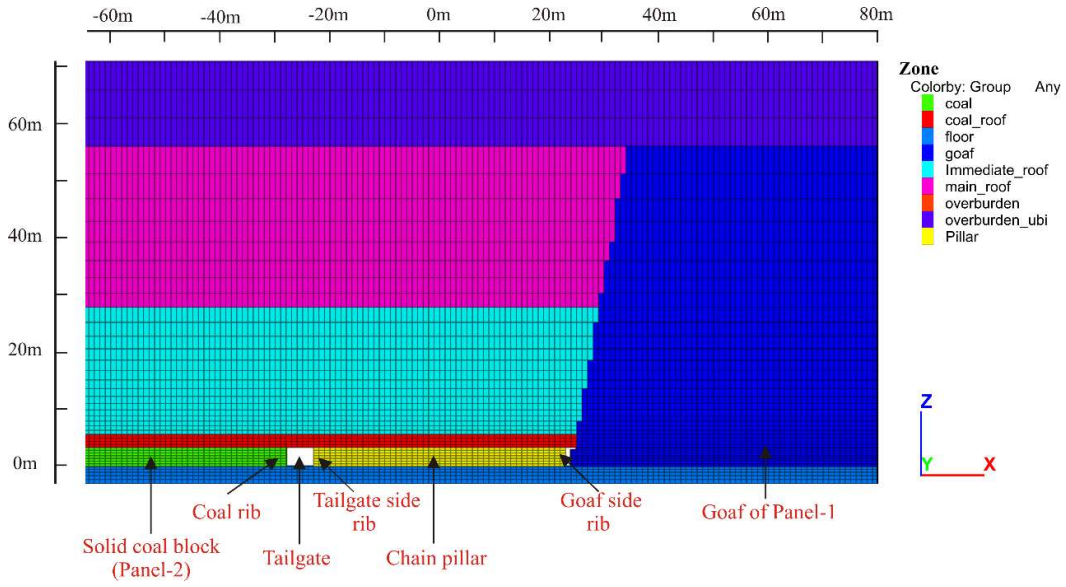

Figure 9.9 Terminology used to locate the study point and describe the distribution of vertical stress and failure in the chain pillar

Figure 9.9 presents the terminology used for describing the modelling results in terms of the distribution of vertical stress and failure in the chain pillar. The rib of the chain pillar adjacent to the extracted first panel is termed as 'goaf side rib', while the rib adjoining the tailgate of the unmined second panel is termed as 'tailgate side rib'. The rib of the solid coal block of the second panel is termed as 'coal rib'.

Figures 9.10 (a)-(d) show the block contour of vertical stress for different pillar widths. The maximum vertical stress is observed in the immediate roof in all the cases. At the seam level, the maximum vertical stress in the 50 m wide pillar is concentrated 4 m inside the tailgate side after mining of the first panel and at the pillar centre when both the panels were mined. A similar stress distribution pattern is observed for the 60 m wide pillar. For the 70 m wide chain pillar, the maximum vertical stress is concentrated at two locations in the pillar: at 3 m depth from the tailgate side and 13m from the goaf side when the first panel was mined. The maximum vertical stress is skewed towards the second panel when both the panels are mined. For the pillar width of 80m, the concentration of the maximum vertical stress was between 12-

15 m inside the goaf side pillar rib when the first panel was mined. A sharp peak is seen at 3 m inside the tailgate side rib due to the combined effect of side abutment loading due to mining the first panel and loading due to the gate road development. When both the panels are mined, a relatively uniform distribution of vertical stress is noted at 16 m inside the pillar edge of the second panel and 26 m inside the pillar edge of the first panel.

Figures 9.11 (a)-(c) show the failure in the chain pillar and the surrounding strata at the different stages of loading. The rib of the 50m wide pillar received failure up to 2 m from the edge after the development of gate roads. While tensile failure was observed at the mid-height of the pillar rib, a majority of the zones received shear failure. The failure extended to 3 m inside the tailgate side pillar rib when the first panel was mined for all the studied pillars. The depth of failure in the goaf side pillar rib extended up to 6 m from the edge, whereas the immediate roof above the pillar from the goaf side underwent shear failure up to 18 m inside the edge due to side abutment loading of the first panel. The depth of failure in the goaf side pillar rib was limited to 3 m and 6 m at the bottom and top ends of the pillar. A significant portion of the elastic core remained in the pillar, and most of the immediate roof was intact in all the cases after the mining of the first panel.

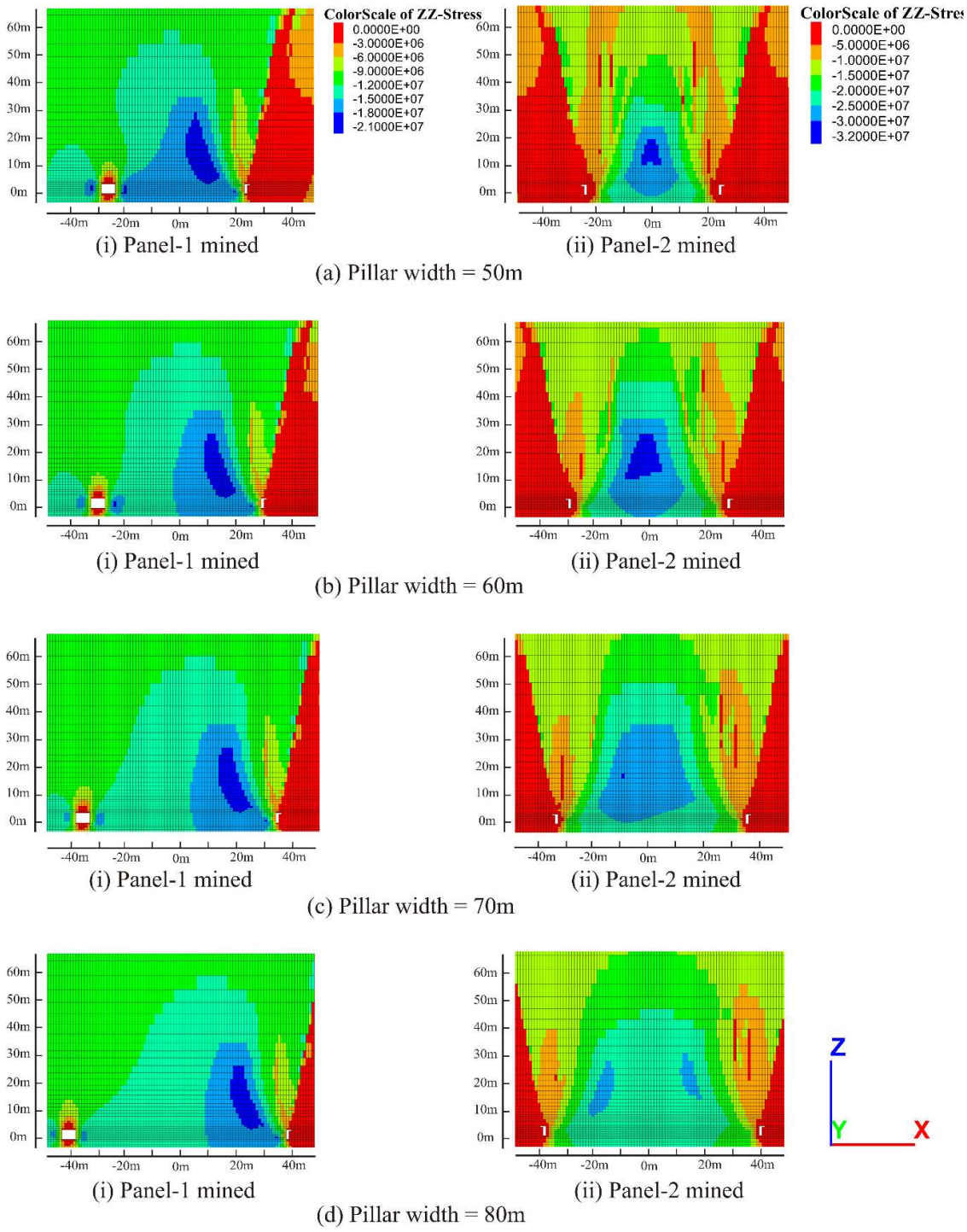

Figure 9.10 Block contour of vertical stress distribution with (i) one-sided goaf (P1 mined) and (ii) both-sided goaf (P1P2 mined) for pillar width of (a) 50, (b) 60, (d) 70, and (d) 80 m

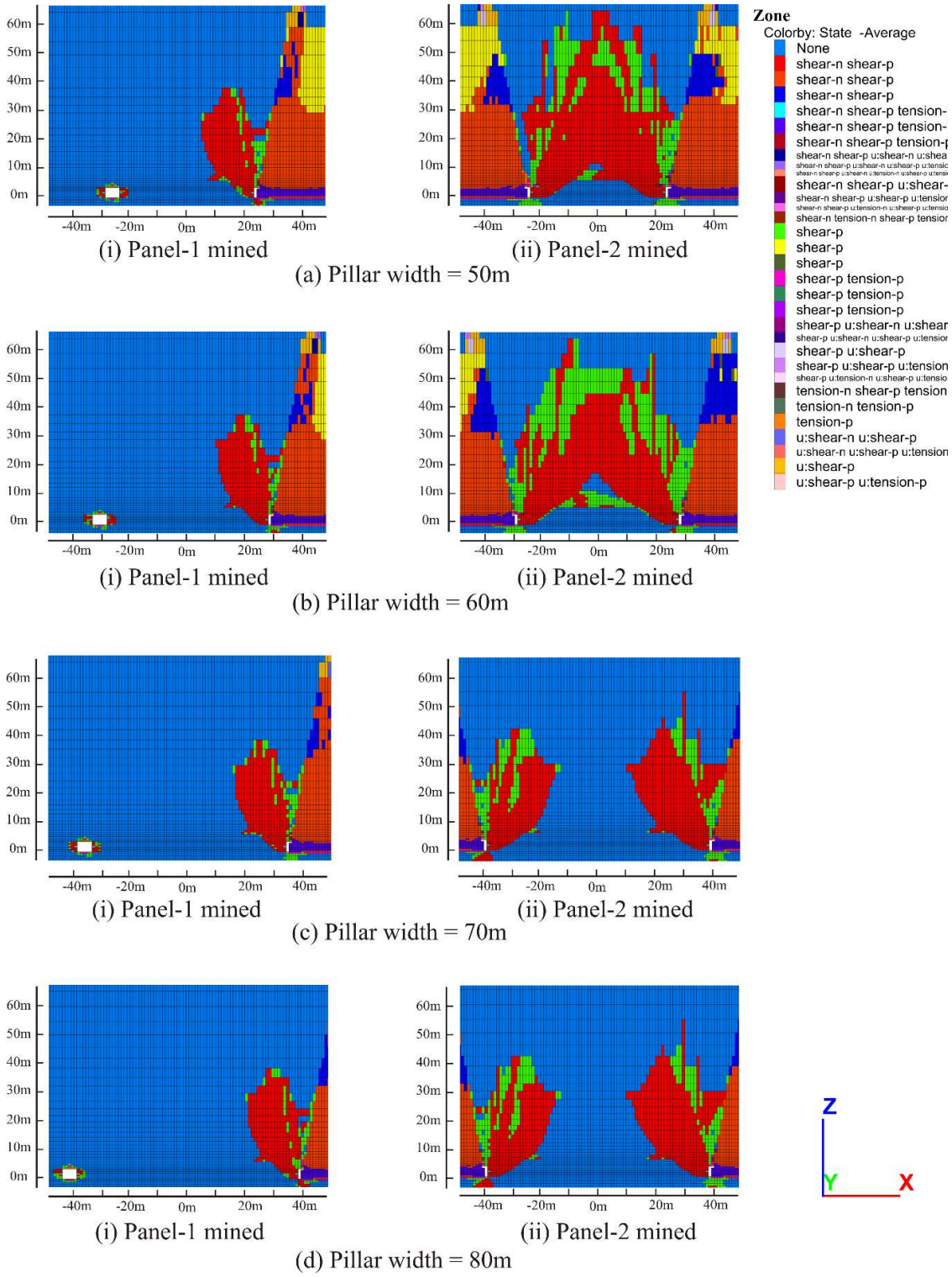

Figure 9.11 Failure in the chain pillar with (i) one-sided goaf and (ii) both-sided goaf for pillar width of (a) 50, (b) 60, (d) 70, and (d) 80 m

After mining the second panel, the failure in the pillar ribs extended up to 9-10 m inside the edge for all four cases. While the failure depth was limited to 6 m at the bottom end, it reached up to 10 m at the top end of the pillar for widths of 50 m and 60 m because of lower confinement provided by the weak immediate roof. The extent of failure at the pillar bottom and top ends for both the 70 m and 80 m wide pillars was limited to 4 m and 9 m, respectively.

The immediate roof above the 50 m and 60 m wide pillars failed completely. However, about 25-35 m core of the 50 - 60m wide chain pillar remained intact. For the 80 m wide pillar, the failure was limited to only the roof above the pillar ribs, and the 20m wide roof above the pillar core was intact. The roof in the roof of the 70m wide pillar was very limited and was noted 20m above the pillar. The intact core of 47 - 57m width was noted for 70 - 80m wide pillars.

Figures 9.12 (a)-(c) show the rotation of stress tensor around the excavation, resulting in a different level of confinement at the excavation boundary. Upon the development of the gate roads, the confinement improved towards the pillar core as well as towards the roof and floor. The confinement provided by the floor was substantially greater than the roof due to the relative difference in their stiffness, although it was almost negligible at the mid-height of the pillar edges (Figure 9.12a).

After the extraction of the first panel, the confining stresses in 1-2m wide ribs of the pillar were negligible. The major confinement in the goaf side rib of the pillar developed due to the presence of the stronger floor at 3-5 m from the edge (Figure 9.12b). However, the confining stresses increased to the maximum value at the pillar-roof contact at 5-7m depth in the rib. This is primarily due to an 18 m deep failure in the weak immediate roof from the goaf side panel edge and low abutment angle. The stronger floor was able to provide substantial confinement during the course of loading. The vertical stresses were redirected towards the tailgate side of

the pillar rib, leading to the concentration of the maximum principal stress at 3-4m in the tailgate side rib due to confinement provided by the floor and the intact immediate roof.

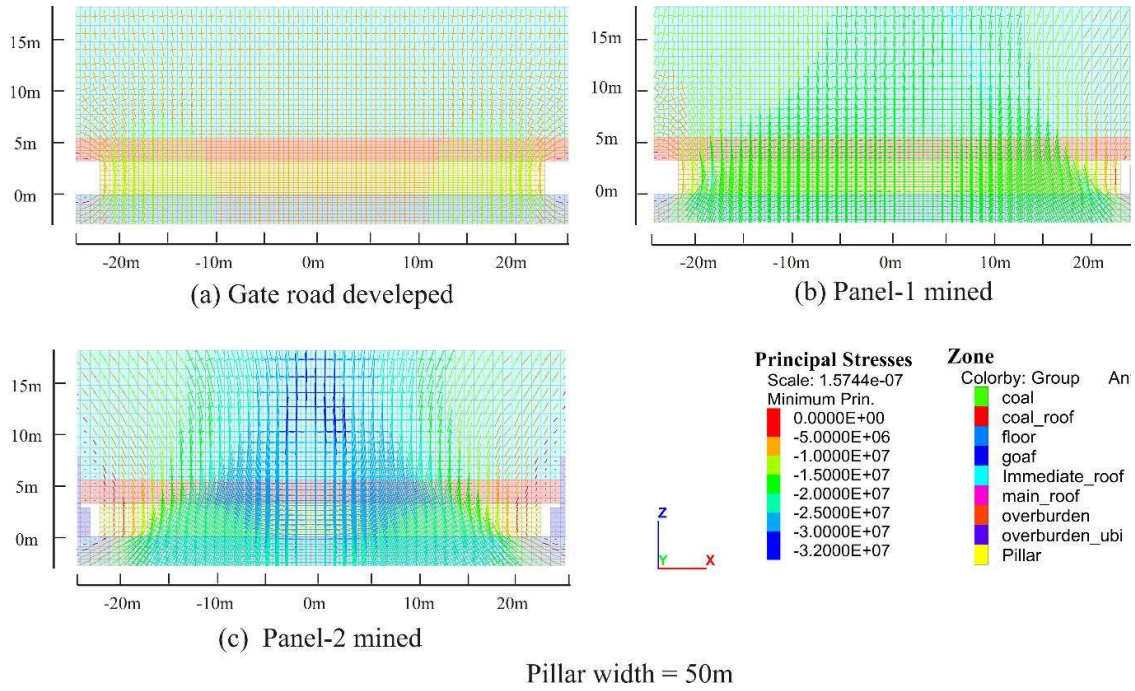

Figure 9.12 Principal stress tensor plot showing confining stress for the pillar width of 50 m after (a) the development of gate roads, (b) mining of the first panel, and (c) mining of both the adjoining panels

Figure 9.12 (c) shows the redistributed stress trajectory after extraction of both the adjoining panels. The strong floor was able to provide substantial confinement in the core zone of the pillar at this stage of loading. The confining stresses in 2-3 m wide ribs of the pillar were negligible. The substantial confining stresses in the pillar at the roof-pillar contact were realised at 5-6m from its edges due to failure in the immediate roof.

The model observed convergence between roof and floor of the gate road was 22 mm against the field observation of 15-25 mm. Figure 9.13 shows the convergence between the roof and the floor in the tailgate and the lateral deformation of the solid coal rib and pillar rib in the second panel after the extraction of the first panel. The maximum roof-floor convergence was

89 mm for the pillar width of 50 m, while the minimum convergence of 71mm was noted for the 80 m wide pillar. The field observations showed that the convergence between roof and floor varied between 80-110 mm for the pillar width of 50m. With every 10m increment in the pillar width, the convergence decreased by 5mm for the chain pillar width of 50-70m in the model. The pillar rib produced the maximum side closure of 58mm for the 50m wide pillar and the minimum closure of 42 mm for the 80m wide pillar. The maximum coal rib closure was 18 mm, while the minimum closure was 13 mm for pillar widths of 50m and 80m, respectively.

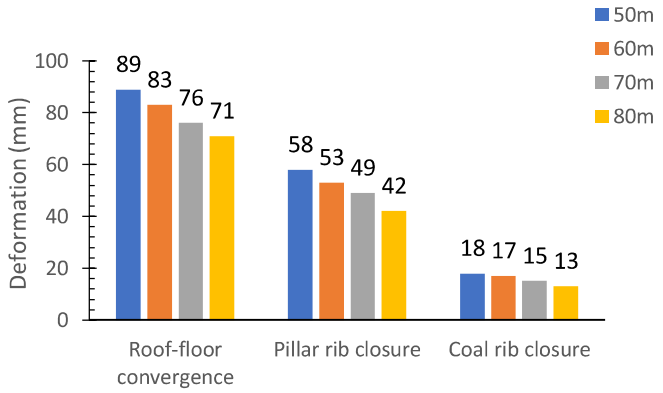

Figure 9.13 Model observed convergence in the tailgate and lateral deformation in the coal and pillar ribs of the second panel for pillar widths of 50, 60, 70, and 80 m

9.4.2 P2-P3 Chain pillar in Adriyala Seam-I Working

Figures 9.14 (a)-(c) show the distribution profile of average vertical stress for optimum pillar width of 56 m and the pillar width of 63 m as implemented in the field. The in-situ vertical stress of 10.6 MPa was uniformly distributed before any excavation in the seam. After development, peak vertical stress of 15.1 MPa developed in the ribs of the pillars. After extraction of the first panel, a sharp peak of 21.6 MPa and 20.5 MPa was observed at the tailgate side of 56 m and 63 m wide pillars. The peak side abutment stress ranged from 1.93 - 2.04 times the in-situ vertical stress. The maximum stress recovery of 8.6 MPa (81.2% of the in-situ

stress) in the goaf was noted at a distance of 60 m (0.12H) from the panel edge in both cases at this stage. When both the adjoining panels were mined, the stress profile of these pillars formed a single peak located at the pillar centre. The peak vertical stress was 28.5 and 29.3 MPa for pillar widths of 56 m and 63 m, respectively. The maximum goaf stress recovery in both the panels reached the in-situ stress at this stage.

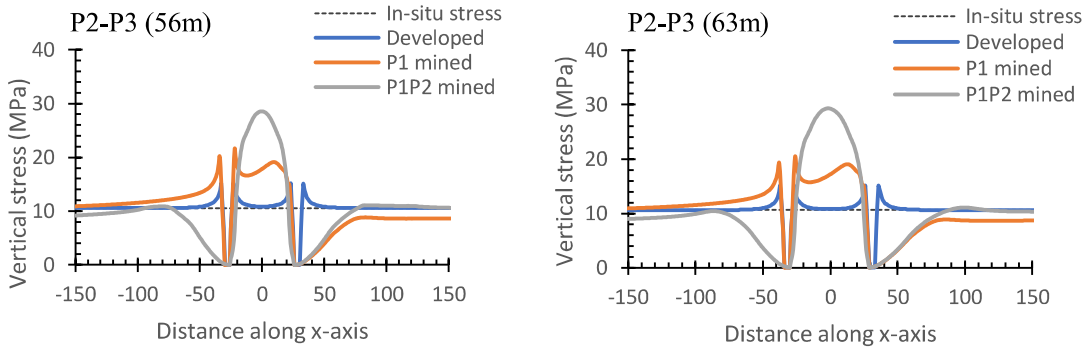

(a) (b)

Figure 9.14 Distribution of vertical stress in the chain pillars of (a) 56 and (b) 63 m width

The observed failure and vertical stress profile in these pillars and the surrounding strata were similar to that in 50-60 m wide chain pillars between the panels P1-P2 of the same mine as described in the previous section. The ribs of these pillars failed up to 3 m inside the pillar edge after the development of the gate roads. Tensile failure was observed at the mid-height and shear failure at the rest part of the pillar ribs. The failure extended to 4 m in the tailgate side pillar rib and up to 8 m in the goaf side rib of the pillars upon mining of the first panel. The extent of failure in the goaf side rib of these pillars at the floor and roof horizons were 4m and 8m, respectively, owing to the presence of relatively weaker roof layers. The shear failure in the immediate roof penetrated up to 20 m from the goaf side edge at this stage of loading.

After the extraction of the second panel, the failure in the ribs of these pillars extended up to the depth of 12 m from their edges. The failure depth at the bottom and top ends of the pillar

reached up to 6 and 12 m, respectively. The extensive failure at the top end was due to the lower confinement by the relatively weaker immediate roof. The immediate roof above these pillars failed completely. However, the pillar core of 27 m width remained intact in the 56 m wide pillar, while the stable core of 34 m width was noted for the 63 m wide pillar.

The maximum vertical stress was concentrated in the immediate roof at different stages of loading of these pillars. At the seam level, the maximum vertical stress was located 4 m inside the tailgate rib of the pillars upon mining the first panel, which further shifted to their core upon mining both the panels. The floor strata provided greater confinement in comparison to the relatively weaker immediate roof strata at the development stage. The confinement due to the immediate roof was reduced further due to the low abutment angle and failure in the roof at the subsequent stages of loading.

Figure 9.15 presents the convergence in the tailgate and the lateral deformation of the solid coal rib and the pillar rib. The gate road convergence of 92-98 mm was noted for pillar width of 63-56 m. The lateral deformation in the pillar and coal ribs were 69-63 mm and 25-24 mm.

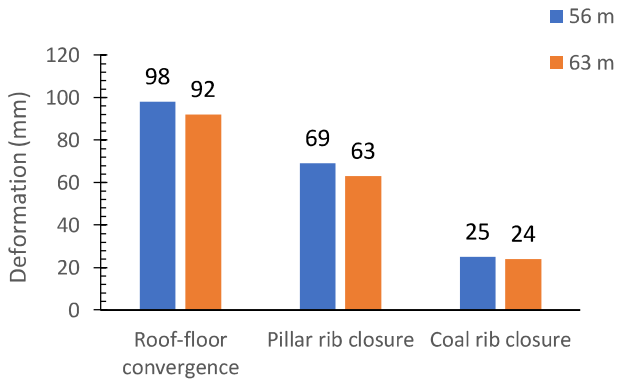

Figure 9.15 Model observed convergence in the tailgate and lateral deformation in the coal and pillar ribs of the second panel for chain pillar widths of 56 and 63 m

9.4.3 Chain Pillar between panels P3-P4 in Adriyala Seam-I Working

Figures 9.16 (a)-(b) show the vertical stress profile for optimum pillar width of 60 m and field pillar width of 69 m. The in-situ vertical stress of 11.6 MPa was uniformly distributed prior to any excavation in the seam. After the development of the gate roads, the peak vertical stress of 16.3 MPa was observed near the ribs of the pillars. When the first panel was extracted, a sharp peak of 23.1 - 22.2 MPa was observed at the tailgate side rib of 60 m and 69 m wide pillars. The peak side abutment stress was 1.9-2.0 times the in-situ vertical stress. The maximum stress recovery of 9.84 MPa (85% of the in-situ value) was attained in the caved goaf at a distance of 60 m (0.12H) from the panel edge in both cases. After extraction of the adjoining panels, the vertical stress profile of 60 m and 69 m wide pillars formed a single peak of about 31 MPa, located at the pillar centre. The maximum goaf stress recovery in the adjoining panels of the pillars reached the in-situ vertical stress value at this stage of loading.

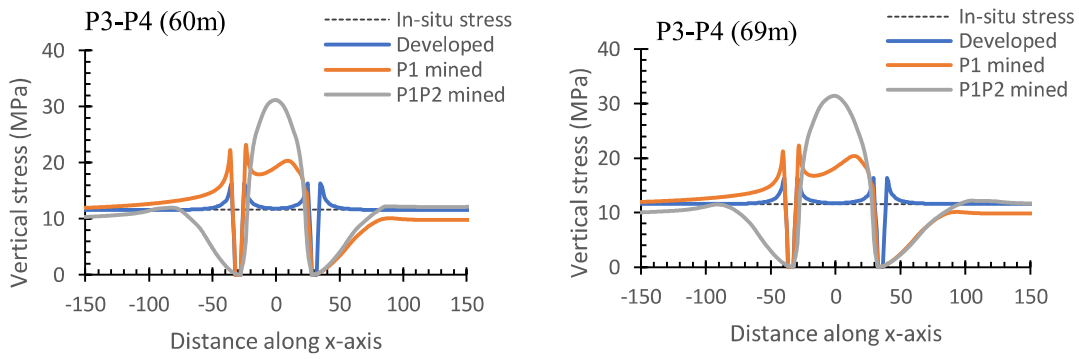

Figure 9.16 Distribution of vertical stress in the chain pillars of (a) 60 and (b) 69 m width

The 3m wide failure that formed along both the sides of the pillar after the development of the gate roads widened to 4 m in the tailgate side rib and up to 8 m in the goaf side rib after the extraction of the first panel for either width of the chain pillar. The extent of failure at the floor and roof horizons was 4 m and 8 m, respectively. The greater extent of failure in the latter case

was due to a relatively weaker immediate roof. The shear failure extended up to 22 m from the goaf edge side of the pillar.

After extraction of the second panel, the failure in the ribs of these pillars extended up to 11 m from their edges. However, the extent of failure at the bottom end was limited to 7 m because of the greater confinement provided by the relatively stronger floor strata. The immediate roof above these pillars failed completely in shear. However, the core of 37 and 46 m wide pillars remained intact for the 60 m and 69 m wide pillars, respectively.

Figure 9.17 shows the convergence and lateral displacement in the solid coal rib and the pillar rib in the tailgate of the second panel after extraction of the first panel. The convergence and pillar rib closure were 98 mm and 70 mm, respectively, for the field size pillar width of 69 m. These values increased by 8 mm for the model estimated optimal width of 60 m.

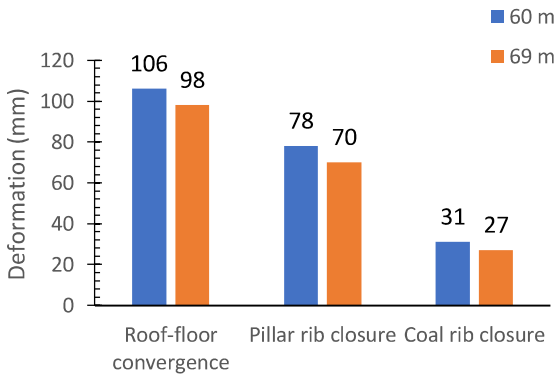

Figure 9.17 Model observed convergence and lateral deformation in the coal and pillar ribs in the tailgate of the second panel for chain pillar widths of 60 and 69 m

9.4.4 Chain Pillars Between Panels A4-A5 in Moonidih XVIII Seam Working

Figures 9.18 (a)-(c) show the distribution profile of the vertical stress for optimum pillar width of 25m along with the 45m wide pillar practised in the field. As the difference in width between the actual and the suggested pillar width was quite significant, an experimental pillar of 35 m width was also studied to cross-check the difference in their overall performance.

Before any excavation, the vertical stress of 7.7 MPa was uniformly distributed in the seam. After the development of the gate roads, the stress redistribution resulted in the vertical stress concentration up to 11.5 MPa in the ribs along the gate roads for the considered pillar widths. Two peaks in the profile of the induced vertical stress were observed upon mining the first panel. The peak vertical stress in the pillar was 17.7, 16.9, and 16.6 MPa for 25, 35, and 45 m wide pillars, respectively. The peak side abutment stress ranged from 2.16 - 2.30 times the in-situ vertical stress, and it was located at the goaf side pillar rib in all the cases. The maximum stress recovery of 4.19 MPa (54.3 % of the in-situ value) was achieved in the goaf at 34 m (0.1H) from the panel edge in all three cases.

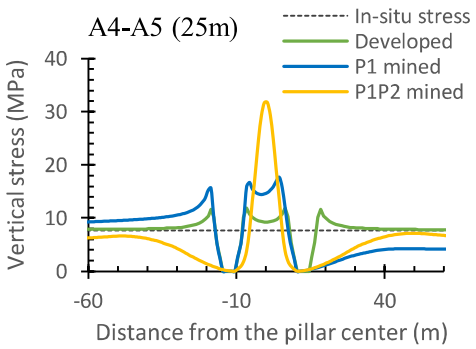

(a)

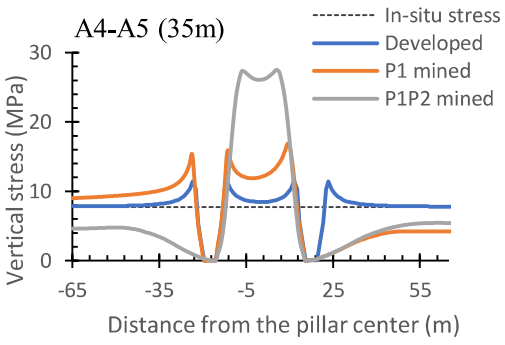

(b)

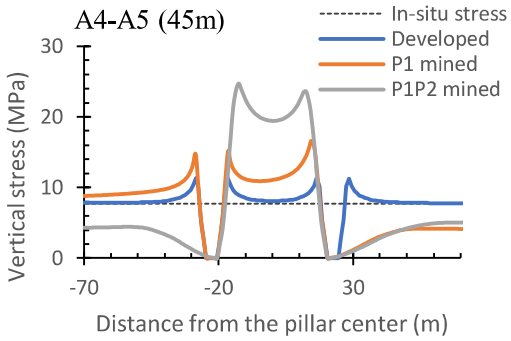

(c)

Figure 9.18 Distribution of vertical stress in the chain pillars of (a) 25, (b) 35 and (c) 45 m width

When both the adjacent panels were mined, the stress profile in the pillar showed a single peak of 31.7 MPa for the 25 m wide pillar. On the other hand, the 35 m and 45 m wide pillars showed double peaks of 27.2 and 24 MPa in their vertical stress profiles. These peaks were located on either side of the pillar at 5.5 and 12.5 m from the centre of the pillars. The maximum goaf stress in the second panel was 84, 60, and 57% of in-situ stress, while it increased to 92, 71, and 66% of the in-situ stress in the first panel while working with the chain pillars of 25, 35, and 45 m width.

Figures 9.19 (a)-(c) show the failure in the pillar and the surrounding strata at different stages of loading. The rib of the pillar received failure up to 3 m inside the edge after the development of gate roads. The failure extended to 4 m in the tailgate side rib after extraction of the first panel. The failure depth extended to 6 m for 25 m and 35 m width pillars and up to 5 m in the 45 m wide pillar. The immediate roof in the goaf side pillar rib received shear failure over 6m width and 10m height due to side abutment loading of the first panel. The failure depth was limited to 4 m at the pillar bottom. Approximately 10, 20, and 30 m elastic core remained in the 25, 35, and 45 m wide pillars, respectively. Most of the immediate roofs above these pillars were intact after mining the first panel.

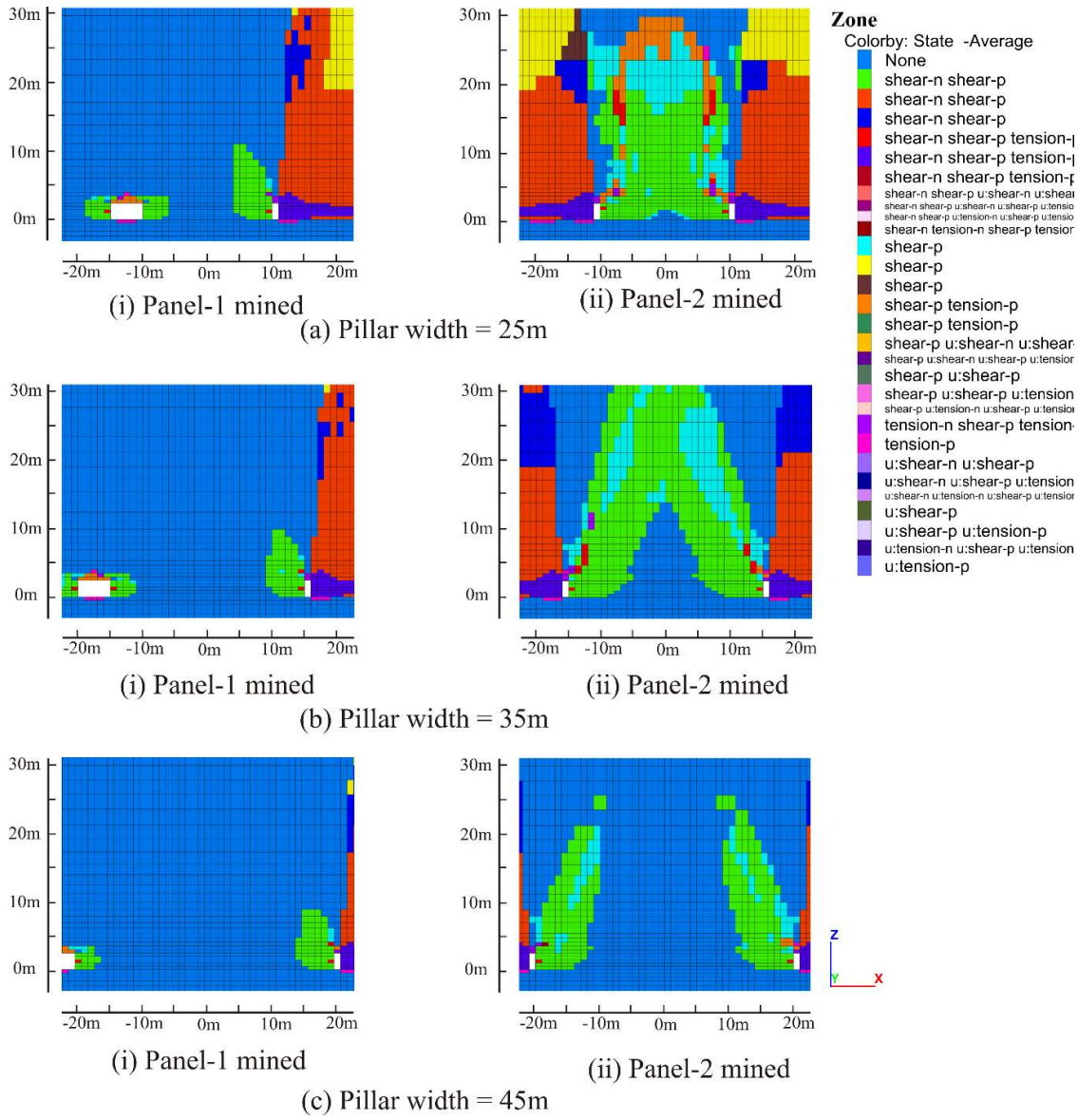

Figure 9.19 Failure state of the pillar system with (i) one-sided goaf and (ii) both-sided goaf for pillar widths of (a) 25, (b) 35, and (c) 45 m

Upon mining the second panel, the failure reached the core of the 25 m wide pillar, whereas the failure in the ribs extended up to 9-10 m for pillar widths of 35 and 45 m, respectively. While the failure depth was limited to 5-6 m at the bottom end of the pillar, it reached 9-10 m at the top end because of lower confinement in the presence of the coal layer in the immediate roof. The entire immediate and main roof-1 above the 25 m wide pillar failed in shear. Upon

second abutment loading of the pillar width of 35 m, the shear failure in the roof above the failed ribs propagated to get interconnected at 12 m height in the roof. However, for the 45m wide chain pillar, the shear failure in the roof got arrested to 20 m in the roof strata and 8 m rib. Pillar cores of 16 m and 24 m widths remained intact in the pillars of 35 and 45 m width, respectively.

Figures 9.20 (a)-(c) show the plot of vertical stress block contour for the different pillar widths. The maximum vertical stress was concentrated in the coal pillar at both the stages of loading for all cases, except the 35 m wide pillar, which experienced the maximum vertical stress in the immediate roof during the second side-abutment loading. At the seam level, the vertical stress was concentrated 4-5 m inside the tailgate side rib and 6-8 m from the goaf side rib when the first panel was mined. The maximum vertical stress was located at the centre of the 25 m wide pillar when both the panels were mined, whereas it was concentrated at 8-11 m from the edges of the 35 m wide pillar and 5-8 m from the edges of the 45 m wide pillars.

Figures 9.21 (a)-(c) show the plot of stress rotation around the excavation, resulting in a different level of confinement at the excavation boundary at different stages of loading for the pillar width of 25 m. After the development of the gate roads, the confining stress was least at the pillar mid-height in the ribs and increased at a further distance inside the pillar edge. The confinement at the pillar centre was higher compared to the zones near the roof and floor. The confinement provided by the sandstone floor was more significant than the 2.4m thick coal roof.

Upon the first panel mining, substantially greater confinement was provided by the sandstone floor in the goaf side rib of the pillar in comparison to the failed immediate roof (Figure 9.21b). The major confinement in the tailgate side rib of the pillar was due to the intact immediate roof.

The confining stress in the pillar core was primarily due to the stronger floor. The confining stresses in 1 m wide ribs of the pillar were negligible.

When both the panels were mined, the pillar was able to retain significant residual strength due to the confining stress owing to a greater w/h ratio and interface effect (Figure 9.21c). The yielded mass in the ribs and the intact floor provided substantial confinement to the pillar core.

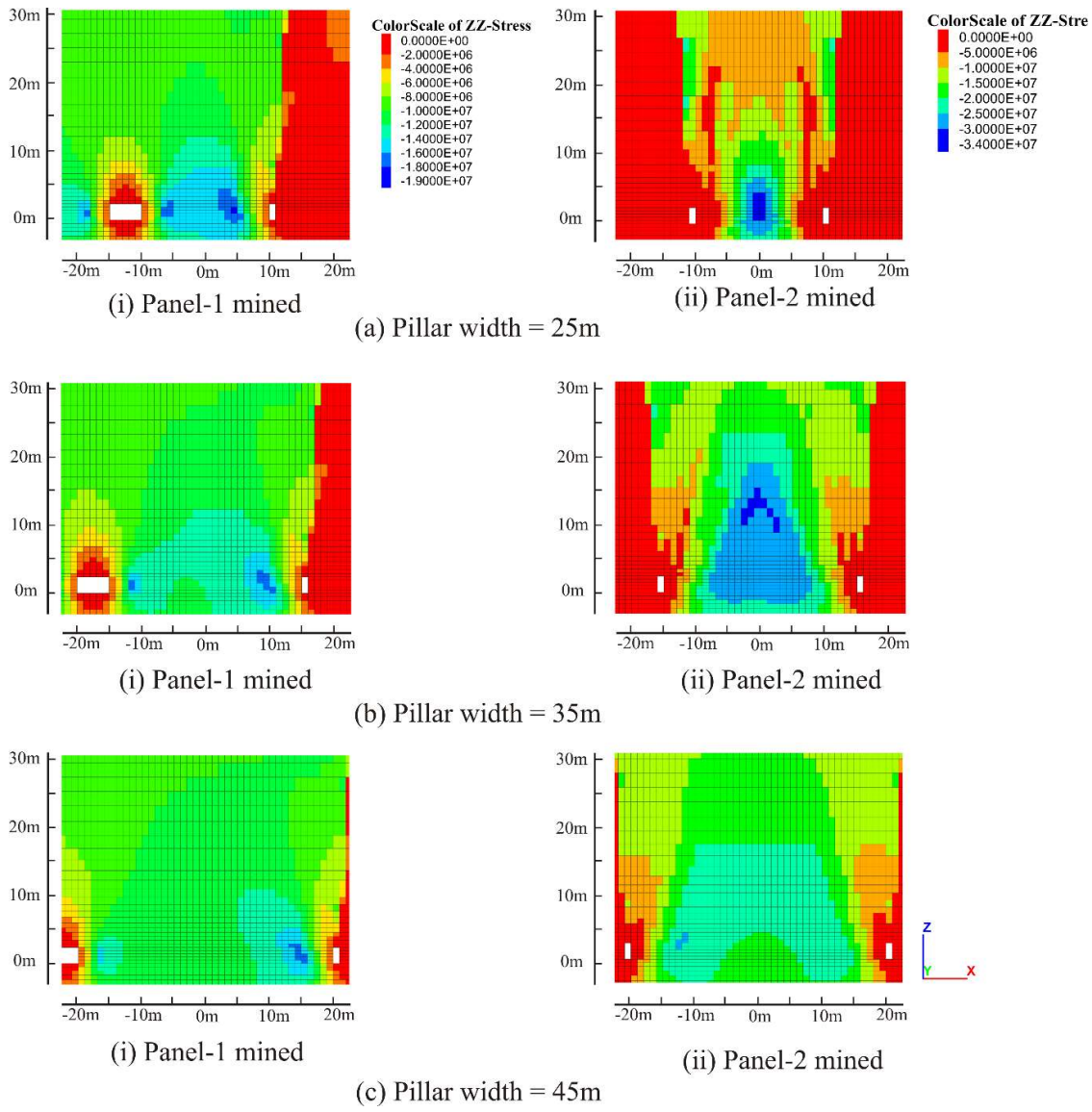

(i) Panel-1 mined (ii) Panel-2 mined

(a) Pillar width = 25m

(i) Panel-1 mined (ii) Panel-2 mined

(b) Pillar width = 35m

(i) Panel-1 mined (ii) Panel-2 mined

(c) Pillar width = 45m

Figure 9.20 Block contour of vertical stress distribution with (i) one-sided goaf and (ii) both-sided goaf for pillar widths of (a) 25, (b) 35 and (b) 45 m

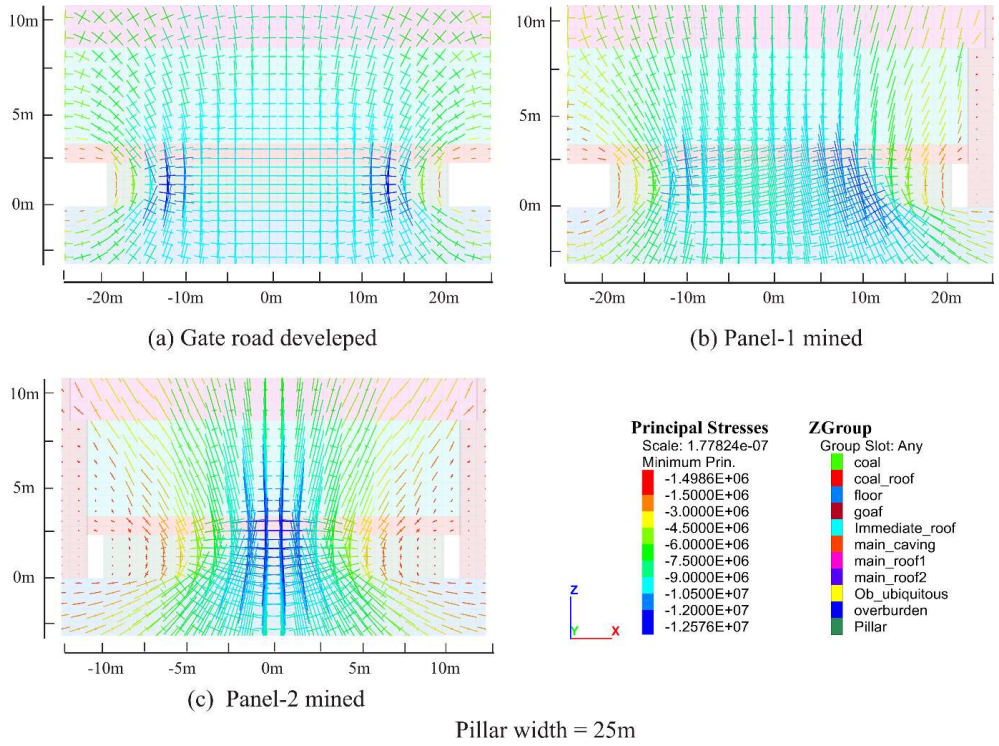

Figure 9.21 Principal stress tensor plot showing confining stress for the pillar width of 25 m after (a) the development of gate roads, (b) mining of the first panel, and (c) mining of both the adjoining panels

Figure 9.22 shows the convergence in the gate road and the closure of the solid coal rib of the second panel after the extraction of the first panel. The gate road convergence was 56 mm, while the lateral deformation in the pillar and coal ribs was 51-52 mm for the optimum pillar size of 25 m. For increased pillar widths of 35 and 45 m, the convergence reduced only marginally to 51 to 52 mm, while the closure of the ribs reduced to 38 to 43 mm. The field observed convergence in the tailgate of the second panel after extraction of the first panel varied between 40 -70 mm.

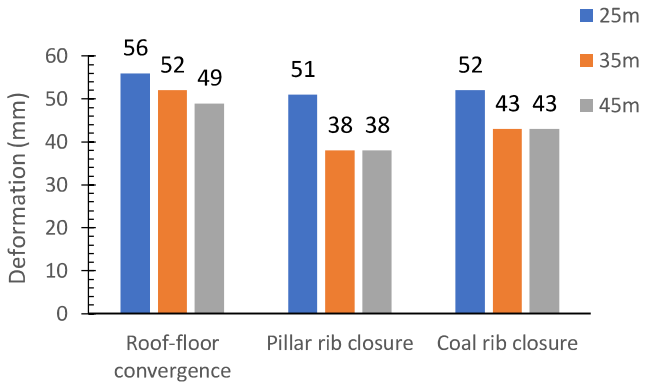

Figure 9.22 Convergence and lateral deformation in the coal and pillar ribs in the tailgate of the second panel for pillars of 25, 35, and 45 m width

9.4.5 Chain Pillars between Panels D12-D13

Figures 9.23 (a)-(b) show the vertical stress distribution profile for the optimum pillar width of 34 m along with the field pillar width of 50 m, as implemented between D12-D13 panels in coal seam XVI of Moonidih Colliery. The development of the gate road led to a vertical stress concentration of 22.4 MPa in the ribs along the gate roads against the in-situ stress of 14.2 MPa for both pillar widths. In the pillar, two peaks in the stress profile were observed along the seam upon mining the first panel. The peak vertical stress in the pillar was 38.2 and 35.2 MPa, marking the peak side abutment stress of 2.5-2.7 times the in-situ vertical stress. The peak abutment stress for 34 and 50 m wide pillars were located at a distance of 7 and 15 m from the centre of the pillars towards the goaf side pillar edge. The maximum stress recovery in the goaf was 10.2 MPa (72 % of the in-situ value) at a 32 m (0.06H) distance from the panel edge in both cases.

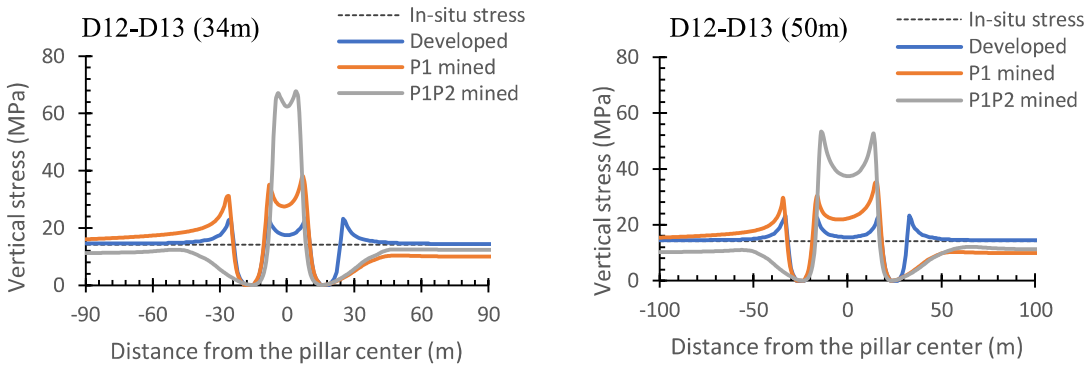

(a) (b)

Figure 9.23 Distribution of vertical stress in the chain pillars of (a) 34 and (b) 50 m width

When both the adjoining panels were mined, the average stress profile in 34m and 50 m wide pillars had a double peak of about 67 MPa and 52.7 MPa, respectively. These peaks were located on either side of the pillar centre at a distance of 4 m and 14 m from the centre of 34 m and 50 m wide pillars, respectively. The maximum goaf stress recovery in the first panel increased to 84-88% of the in-situ stress value for workings for pillar widths of 50 and 34 m, respectively. The maximum goaf stress in the second panel was 75-84% of the in-situ stress in these conditions.

Figures 9.24 (a)-(b) show the failure in the pillar and the surrounding strata at the different stages of loading for these two pillar sizes. The 34 m wide pillar received rib failure to the depth of 6 m from the edges after the development of gate roads. The depth of failure extended to 7 m in the tailgate side rib and 9 m in the goaf side rib after mining the first panel. On the other hand, while working with the 50m wide pillar, the failure depth remained constant in the tailgate side rib and increased to 9 m in the goaf side rib (Fig. 9.24b). The strong sandstone in the immediate roof above the pillar rib remained intact during the side abutment loading of the first panel. Approximately 13 m and 30m elastic core remained in the 34 m and 50 m wide pillars, respectively.

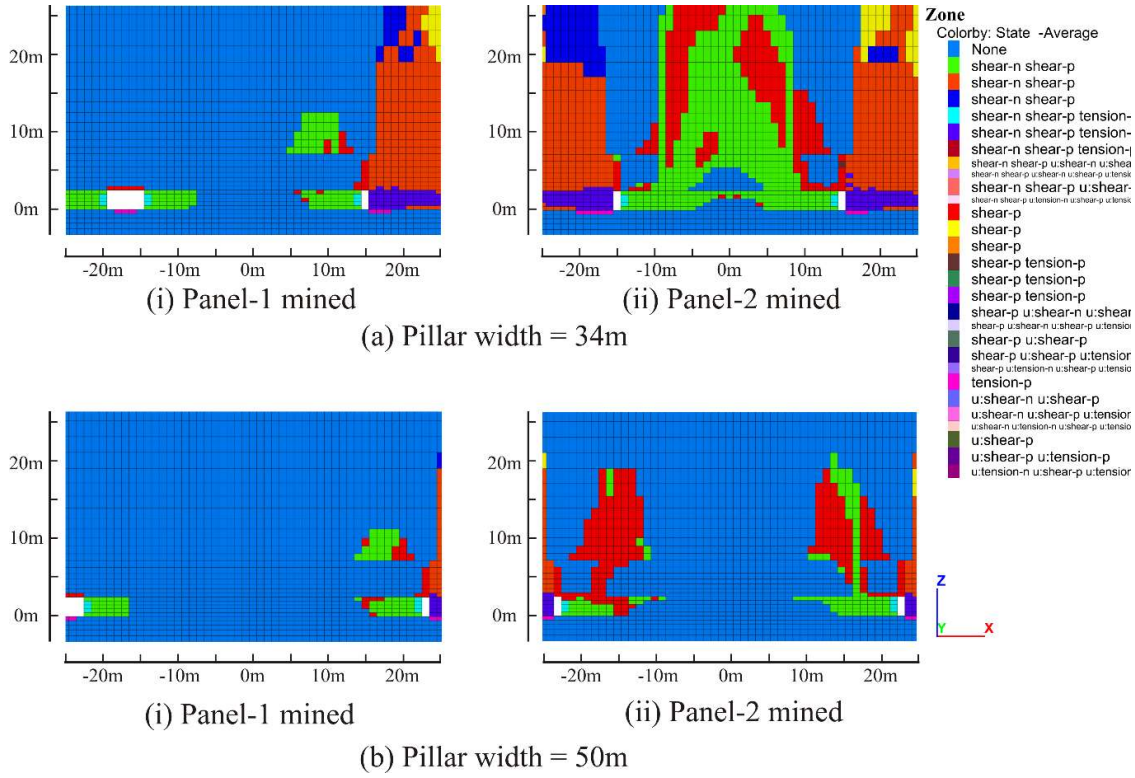

Figure 9.24 Failure state of the pillar system with (i) one-sided goaf and (ii) both-sided goaf for pillar width of (a) 34 and (b) 50 m

Upon mining of the second panel, the failure occurred in the core of the 34 m wide pillar, whereas, for the 50 m wide pillar, it extended up to the depth of 10-12 from the edges. While the failure depth was limited to 9-10 m at the bottom end of the pillar, it reached up to 14 m at the top end because of lower confinement by the immediate roof owing to a very low abutment angle of 4°. The entire immediate roof above the 34 m wide pillar failed in shear. The failure of the immediate roof above the 10-12 m thick failed rib of the 45m wide pillar was limited to 20 m depth. At the bottom end, 8 and 25 m wide cores remained intact for 34 and 50 m wide pillars, respectively.

Figures 9.25 (a)-(b) show the block contour of vertical stress at different stages of loading for the two pillars. The maximum vertical stress was concentrated in the coal pillar except during the second side abutment loading of the 34 m wide pillar, where the maximum vertical stress

was located in the immediate roof. The maximum vertical stress was concentrated 7m inside the edges of the pillars after the development stage. After mining the first panel, the vertical stress was concentrated at 7 m depth in the tailgate rib and 6-9 m in the goaf side rib of these pillars. After extraction of both the panels, the maximum vertical stress shifted to 10-13 m inside the edges for the 34 m wide pillar and 8-11 m for the 50 m pillar.

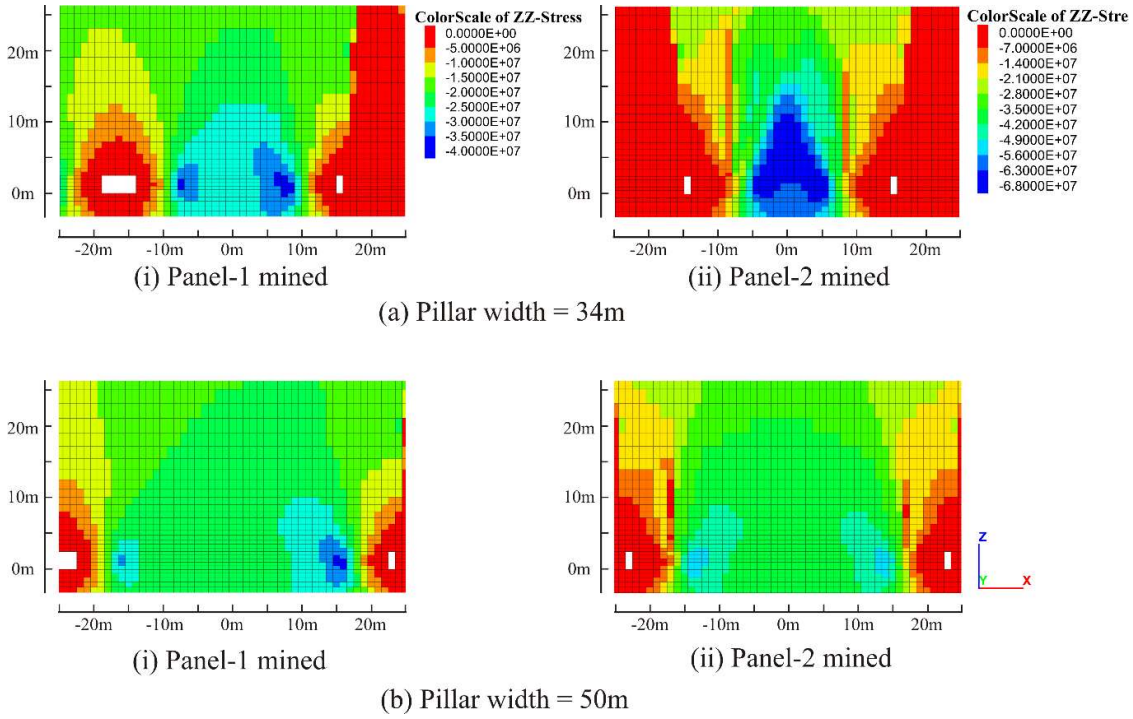

Figure 9.25 Block contour of vertical stress distribution with (i) one-sided goaf and (ii) both-sided goaf for pillar widths of (a) 34 and (b) 50 m

Figures 9.26 (a)-(c) show the plot of stress rotation in and around the 34m wide pillar at different stages of loading. In the pillar ribs, the confining stresses increased towards its core as well as towards the roof and floor. The maximum confining stresses were located 6 - 9 m deep inside the pillar ribs at this stage (Fig. 9.26a).

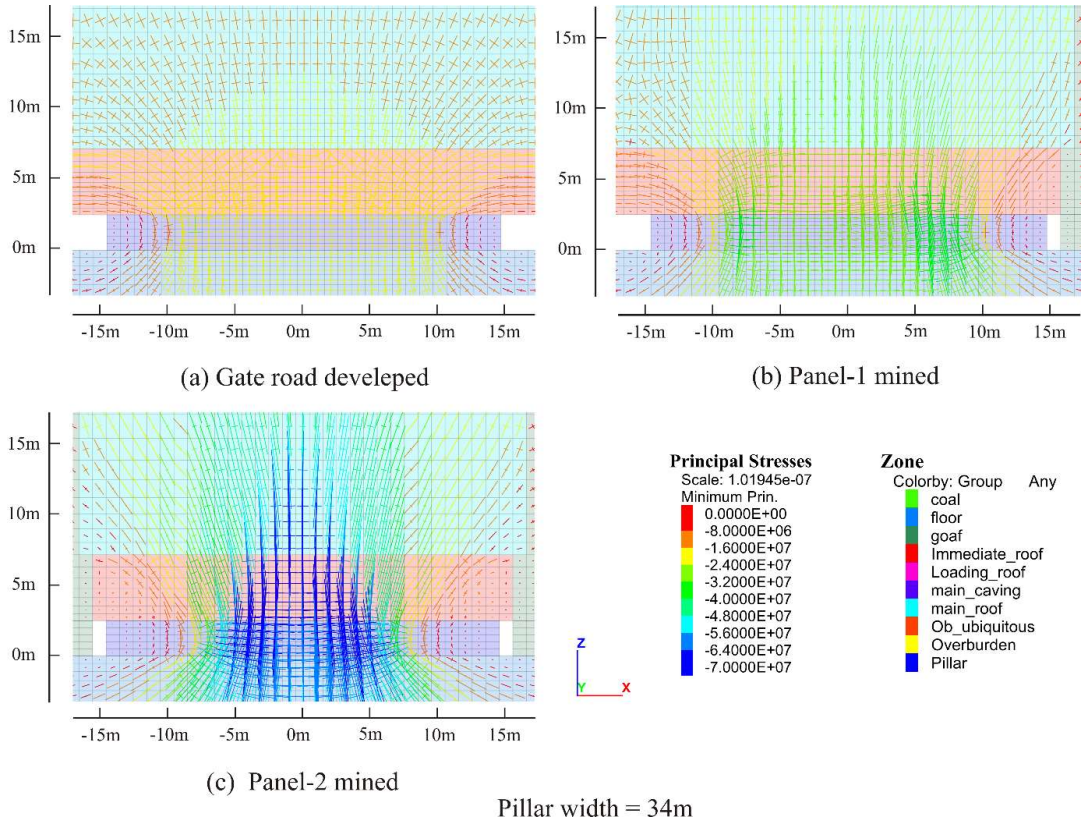

Figure 9.26 Principal stress tensor plot showing confining stress for the pillar width of 34 m after (a) the development of gate roads, (b) mining of the first panel, and (c) mining of both the adjoining panels

Upon mining the first panel (Figure 9.26b), the confining stresses within 1 – 2 m wide goaf and tailgate side ribs of the pillar were negligible. The sandstone floor provided substantially higher confinement in the goaf side rib of the pillar in comparison to the failed immediate roof above it due to the low value of the abutment angle. However, the major confinement along the roof in the tailgate rib of the pillar was noted due to the intact state of the immediate roof. The confining stress in the pillar core was primarily due to the stronger floor.

After mining both the panels, the confining stresses within 2 – 3 m wide ribs of the pillar became negligible. However, the pillar could retain significant residual strength owing to the confining stress because of the considerable w/h ratio and the interface effect (Figure 9.26c).

The yielded coal mass in the ribs, as well as the intact floor, were able to provide substantial confinement to the pillar core.

Figure 9.27 shows the convergence in the tailgate road and lateral deformation of the solid coal rib and the pillar rib of the second panel after the extraction of the first panel. For the field size chain pillar of 50 m width, the gate road convergence was 68mm, while the closure of the pillar and coal ribs was 119 to 130 mm. The field observation showed roof-floor convergence varying between 35-85mm under this condition. The convergence increased by 14 mm, whereas the pillar and coal ribs closure increased by 25 – 26 mm for the optimum pillar width of 34 m. The marginal increase in the convergence and closure with the decrease in the pillar width confirmed that the pillar size implemented in the field could be reduced by 16 m without compromising the stability of the gate roads.

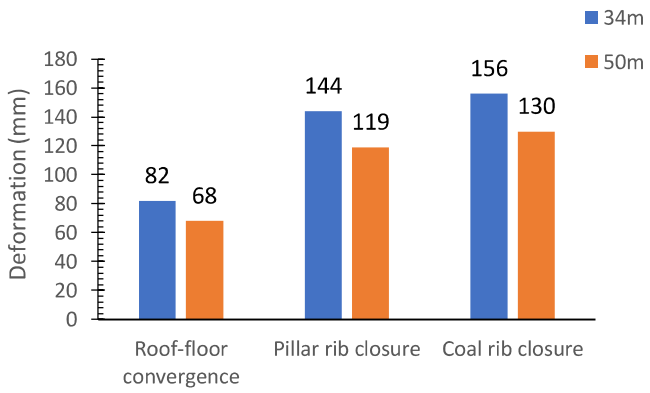

Figure 9.27 Gate road convergence and lateral deformation in coal and pillar ribs of the second panel for pillar widths of 34 and 50 m

9.4.6 Single Row Pillar between Panels T3- T4 in XV Top Seam Working at Moonidih Colliery

Figures 9.28 (a)-(c) show the profile of induced vertical stress for the estimated optimum pillar width of 52 m along with the field size pillar of 60m and experimental pillar width of 70 m between panels T3 and T4 in coal seam XV at Moonidih Colliery. The development of gate

roads led to maximum induced vertical stress of 32.3MPa against the in-situ vertical stress of 20 MPa (Figure 9.28a). Two peaks were observed in the profile of the induced vertical stress upon mining the first panel. The peak vertical stress of 53.5-56.6 MPa was concentrated at 11, 15, and 21 m from the centre towards the goaf side rib of the 52, 60, and 70 m wide pillars, respectively. The peak side abutment stress varied from 2.70-2.83 times the in-situ vertical stress. The maximum goaf stress recovery of 15.1 MPa (75.7% of the in-situ value) was achieved at a distance of 57 m (0.10H) from the panel edge in all three cases.

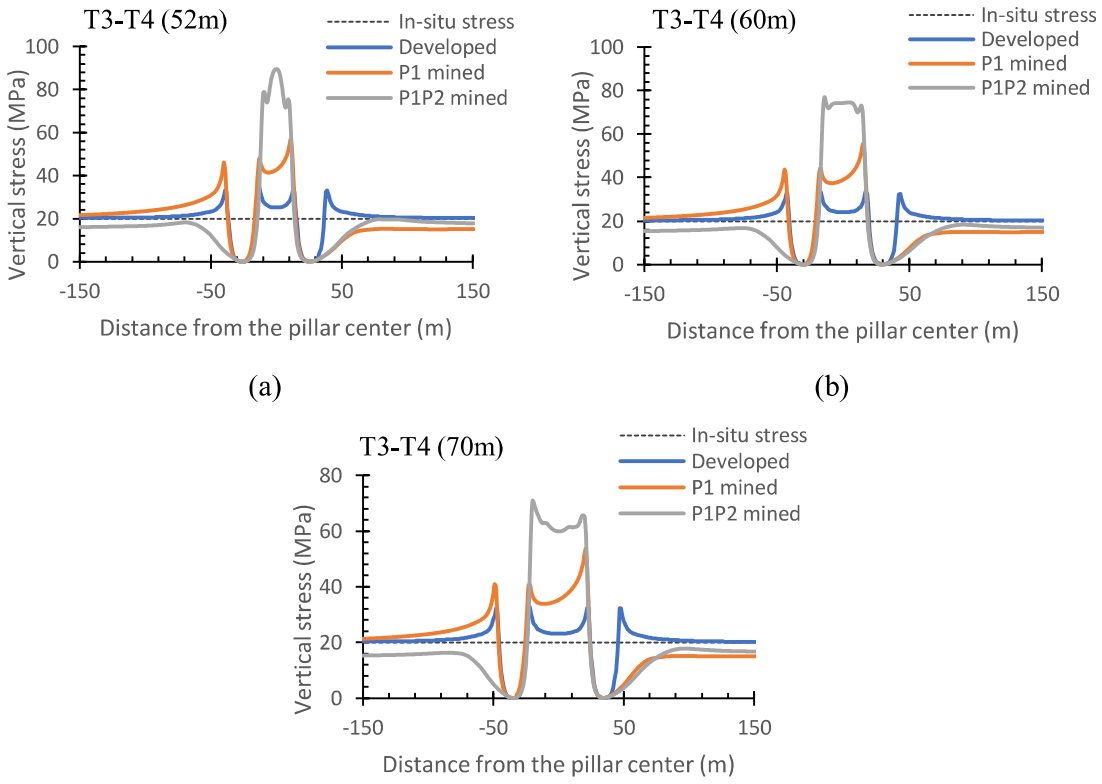

Figure 9.28 Distribution of vertical stress in the chain pillars of (a) 52, (b) 60, and (a) 70 m width

When both the adjoining panels were mined, the vertical stress profile for the optimum pillar width of 52m showed a single peak of 89.5 MPa, whereas the field size pillar width of 60m and the 70 m wide pillar showed two peaks of 76.8 MPa and 70.0 MPa, respectively. These peaks were located on either side of the pillar centre at a distance of 14 m and 20 m from the centre. The maximum goaf stress recovery in the first panel increased to the cover pressure in the working with a pillar width of 52 m, whereas it increased to approximately 88 % of the in-situ vertical stress for workings with pillar widths of 60 and 70 m, respectively. The maximum stress recovery in the second panel was 90, 80 and 75 % of the virgin vertical stress for 50, 60, and 70 m wide pillars, respectively.

Figures 9.29 (a)-(c) show the failure in the pillar and the surrounding strata at different stages of loading for these three pillar widths. The pillars received rib failure up to the depth of 10 m from the edge after the development of gate roads at the cover depth of 865 m. The failure in the 52 m wide pillar extended to 11 m in the tailgate side rib and 13 m in the goaf side rib upon extraction of the first panel. The extent of failure in the 60 and 70 m wide pillars was also similar. A 31 m high vertical fracture was generated in the roof at a distance of 8 m from the goaf side pillar edge in all the cases due to settlement and rotation of the roof in the goaf.

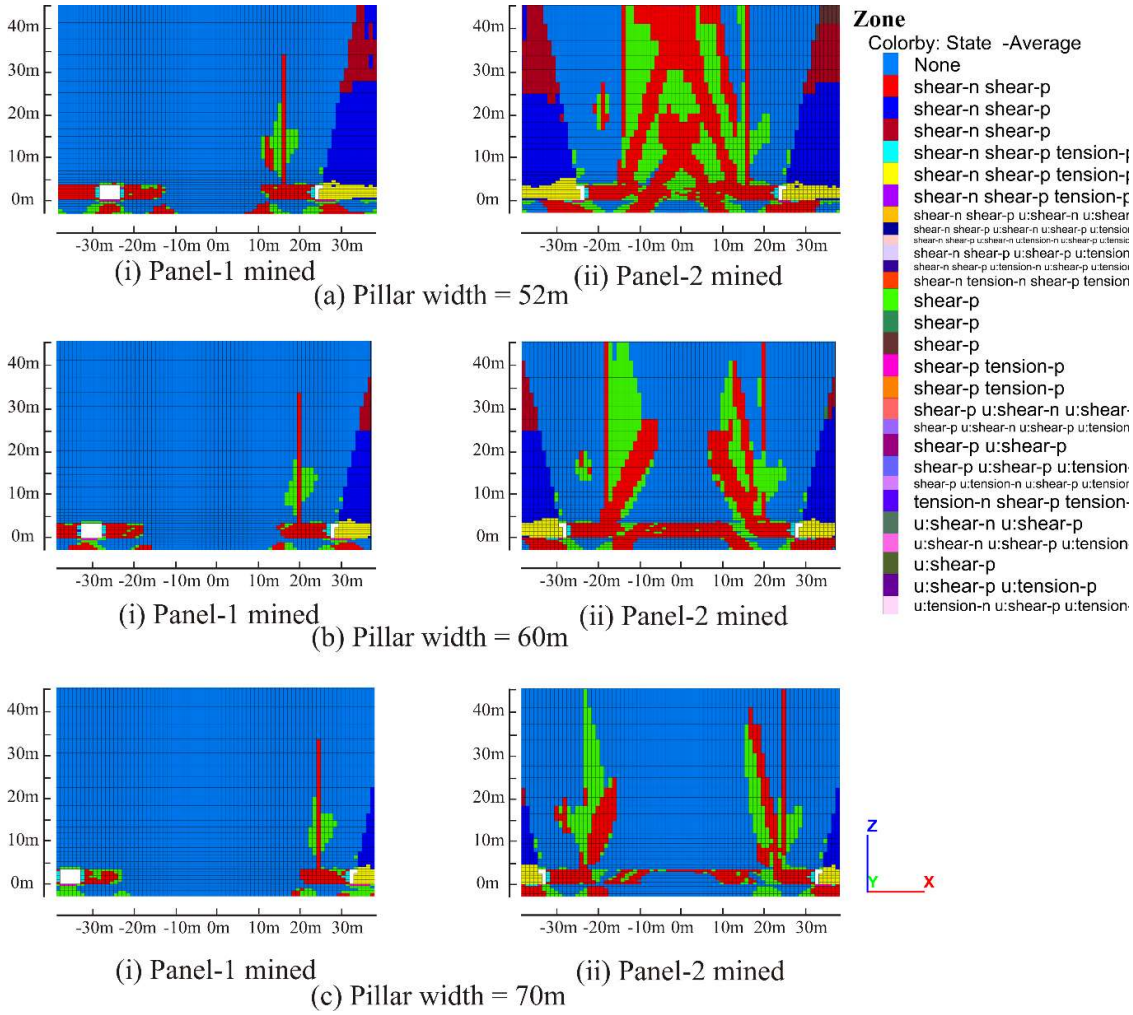

Figure 9.29 Failure state of the pillar system with (i) one-sided goaf and (ii) both-sided goaf for pillar widths of (a) 52, (b) 60, and (c) 70 m

When the second panel was mined, the failure reached the core of 52 and 60 m wide pillars, whereas the failure in the ribs extended up to the depth of 23-25 m for the pillar width of 70 m. While the depth of failure was limited to 24 m at the bottom end of the pillar, it reached up to the core at the top end due to lower confinement provided by the immediate roof owing to a lower abutment angle (11°) in comparison to the floor. The failure in the immediate roof extended up to 32 m, whereas 24 m thick ribs from the edges of 60 and 70 m wide pillars failed

in the horizontal direction. 18 m wide core of the 70 m wide coal pillar remained intact along the bottom end.

Figures 9.30 (a)-(c) show the block contour of the induced vertical stress for the considered pillar widths. The maximum vertical stress was concentrated in the coal pillars at all the stages of loading for different widths. At the development stage, the maximum vertical stress was concentrated at the 9-11 m inside the pillars. The peak vertical stress concentration shifted to 11 m inside the tailgate rib and 12-14 m inside the goaf side rib of these pillars after mining the first panel. After mining both the panels, the maximum vertical stress shifted to the core of the 52 m wide pillar. A uniform distribution of the maximum vertical stress was observed in the 24 m wide core of the 60 m wide pillar. In the 70 m wide pillar, the maximum vertical stress was observed at a distance of 12-14 m from either side.

Figures 9.31 (a)-(c) show the plot of stress rotation around the excavation, causing variation in confining stress in and around the 52 m wide pillar. As the gate roads were developed, the confining stress within 2 m of the ribs at the pillar mid-height became almost negligible. The confinement improved towards the core of the pillar as well as towards the roof and floor. The maximum confining stress was noted at 9-12m inside the pillar ribs.

Upon mining the first panel, the confining stresses within the 2-3 m wide ribs of the pillar in the goaf and tailgate side had a negligible confinement. The stresses increased gradually towards the core zone of the pillar. The sandstone floor provided substantially greater confinement in the goaf side rib of the pillar in comparison to the roof due to the low abutment angle (Figure 9.31b).

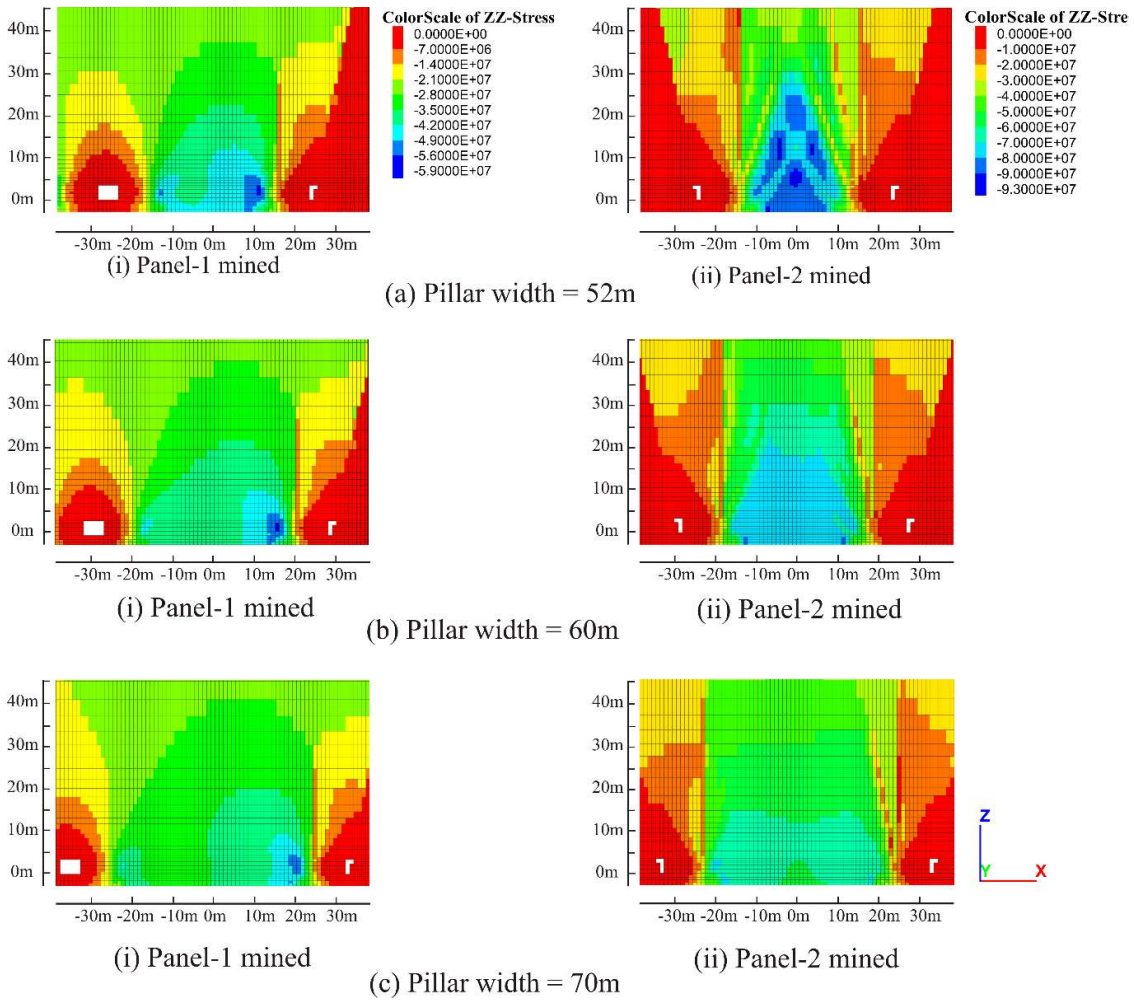

Figure 9.30 Block contour of vertical stress distribution with (i) one-sided goaf and (ii) both-sided goaf for pillar widths of (a) 52, (a) 60, and (c) 70 m

When both the panels were mined, the confining stresses within 3 m wide ribs of the pillars remained negligible. However, the pillar was able to retain significant residual strength owing gradual increase in the confining stress towards its core zone because of the sizeable w/h ratio and interface effect (Figure 9.31c). The yielded coal mass in the ribs and the intact floor provided considerable confinement to the pillar core.

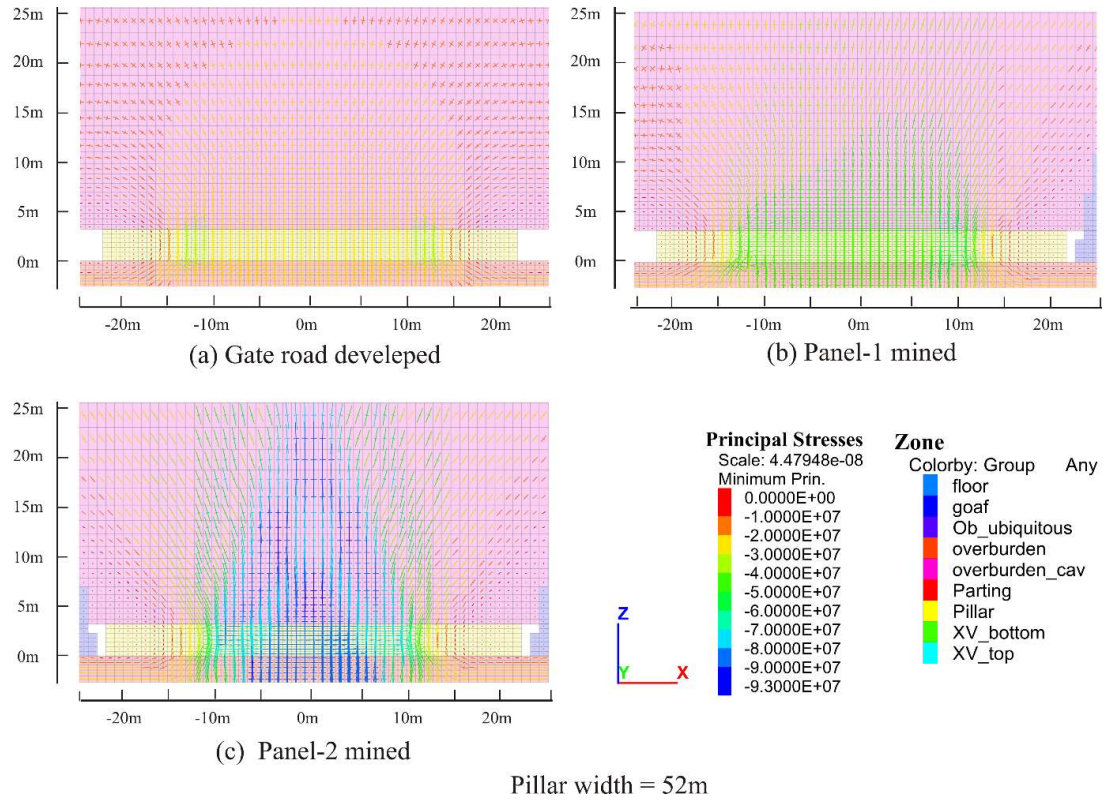

Figure 9.31 Principal stress tensor plot showing confining stress for pillar width of 52 m after (a) development of gate roads, (b) mining of the first panel, and (c) mining of both the adjoining panels

Figure 9.32 shows convergence and lateral deformation of the solid coal and pillar ribs in the tailgate of the second panel. The convergence was significantly lower compared to the closure of the coal and pillar ribs, mainly due to the poor strength of the coal seam and competent sandstone immediate roof. For the field size pillar of 60m width, the convergence in gate road was 168mm, while lateral deformation of the pillar and coal ribs was 453 to 532 mm. The convergence increased by 17 mm, whereas the closure of pillar and coal ribs increased by 41 to 45 mm for reduced pillar width of 34 m. In contrast, the gate road convergence decreased by 16 mm, whereas the ribs closure of solid coal and pillar reduced by 35 to 44 mm for the 70 m wide pillar. The findings showed that the convergence in the gate road is directly related to the pillar width. The pillar size could be reduced by 8 m without any compromise in the design

function of the pillar and the stability of the gate roads, given that proper support measures are taken to contain the deformation in the gate road.

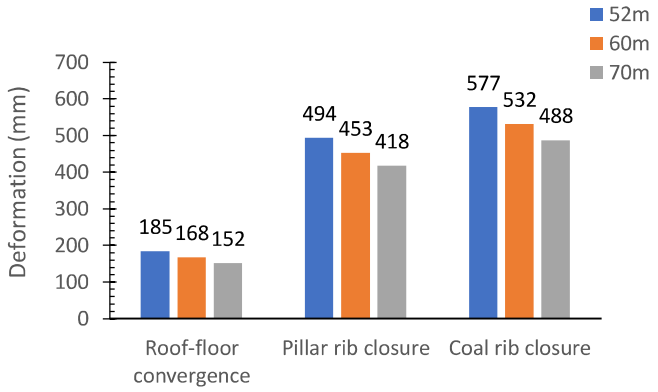

Figure 9.32 The convergence and lateral deformation in the coal and pillar ribs in the tailgate of the second panel for pillar widths of 52, 60, and 70 m.

9.4.7 Double Row Pillar between Panels T3- T4 in XV Top Seam Working at Moonidih Colliery

Considering the difficulty being faced by the mine in effective ventilation of longwall faces in the deep and highly gassy coal seam, another study was done to evaluate the optimal size of pillars for the double row layout. The parametric modelling and soft computing-based model had estimated the optimal pillar width of 42 m for this condition, as discussed in Section 9.1. Figure 9.33 (a) marks the intervening chain pillars and the longwall panels as well as the study point in the chain pillar to describe the modelling results in terms of the distribution of vertical stress and failure in the chain pillar. The rib of the pillars towards the extracted first panel is termed as ‘goaf side rib’, while the rib towards the tailgate of the unmined second panel is termed as ‘tailgate side rib’. The rib of the solid coal block of the second panel is called as ‘coal rib’. The pillar and tailgate entry adjoining the extracted first panel are termed as ‘Pillar 1’ and

'Entry 1', whereas those adjoining the unmined second panel are called as 'Pillar 2' and 'Entry 2', respectively.

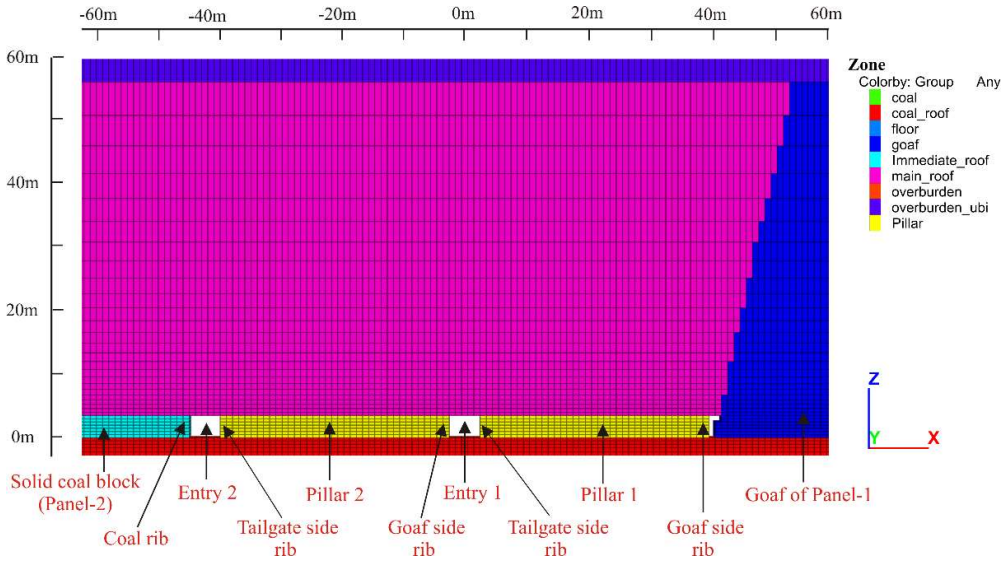

Figure 9.33 Intervening chain pillars and the longwall panels along with the study point in the chain pillar to explain the distribution of vertical stress and failure

Figures 9.34 (a)-(c) show the profile of induced vertical stress for the estimated optimum pillar width of 42 m along with another pillar width of 52 m. The stress redistribution after the gate road excavations led to the concentration of stress up to 35.1 and 33.6 MPa in the ribs along the gate roads for pillar widths of 42 and 52 m. Two peaks were observed for all the considered widths of the pillar.

After extraction of the first panel using 42 m wide pillars, the peak vertical stress of 63.9 MPa was observed in the goaf side rib of Pillar 1 (next to the goaf of the first panel) at the distance of 5 m from its centre, the maximum stress of 55.8 MPa was observed in the goaf side rib of the Pillar 2 (next to the second panel) at a distance of 6 m from its centre.

For 52 m wide pillar, the peak stress of 57.5 MPa was concentrated in the goaf side rib of Pillar 1 at a distance of 10 m from its centre, whereas the maximum stress of 46.8 MPa was observed in the goaf side rib of Pillar 2 at a distance of 12 m from its centre. The maximum stress

recovery in the goaf was 15 MPa (75% of the in-situ stress), which was attained at a distance of 59 m (0.1H) from the panel edge in these cases.

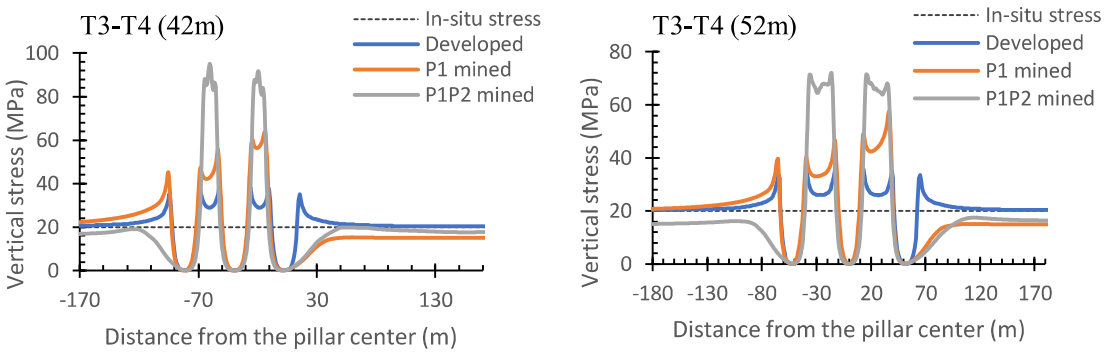

(a) (b)

Figure 9.34 Distribution of vertical stress in the chain pillars of (a) 42 and (b) 52 m width

When both the adjoining panels were mined, the vertical stress profile for the optimum pillar width of 42 m showed a single peak of 91 MPa in Pillar 1 and 95 MPa in Pillar 2. Contrary to these observations, the 52 m wide pillar showed double peaks of 72 MPa, located on either side of the pillar centre at a distance between 7-11m. In the first panel, the goaf stress recovered to the cover pressure with the 42 m wide pillar, while it was 83% of the cover pressure for pillar width of 52 m. The maximum recovery of goaf stress in the second panel was 94% and 77% of the cover pressure in the two cases.

Figures 9.35 (a)-(b) show the failure in the pillar and the surrounding strata at different stages of loading for the experimental pillar widths. The pillars received rib failure up to the depth of 10 m from the edge following the development of the gate roads. For pillar width of 42 m, the depth of failure in the ribs extended to 11-12 m in Pillar 2 and 13-14 m in Pillar 1 (Figure 9.35 (i)-(a)). In the case of 52 m wide pillars, the failure was limited to 10-11m in the ribs of pillar 2 and 12-13 m in Pillar 1. A 35 m high vertical fracture developed in the immediate roof at a

distance of 9 and 8 m from the goaf side edge of Pillar 1 in the case of 42 and 52 m wide pillars, respectively, due to settlement and rotation of the roof in the goaf. Further, the failure width in the floor was limited to the failed ribs in these pillars.

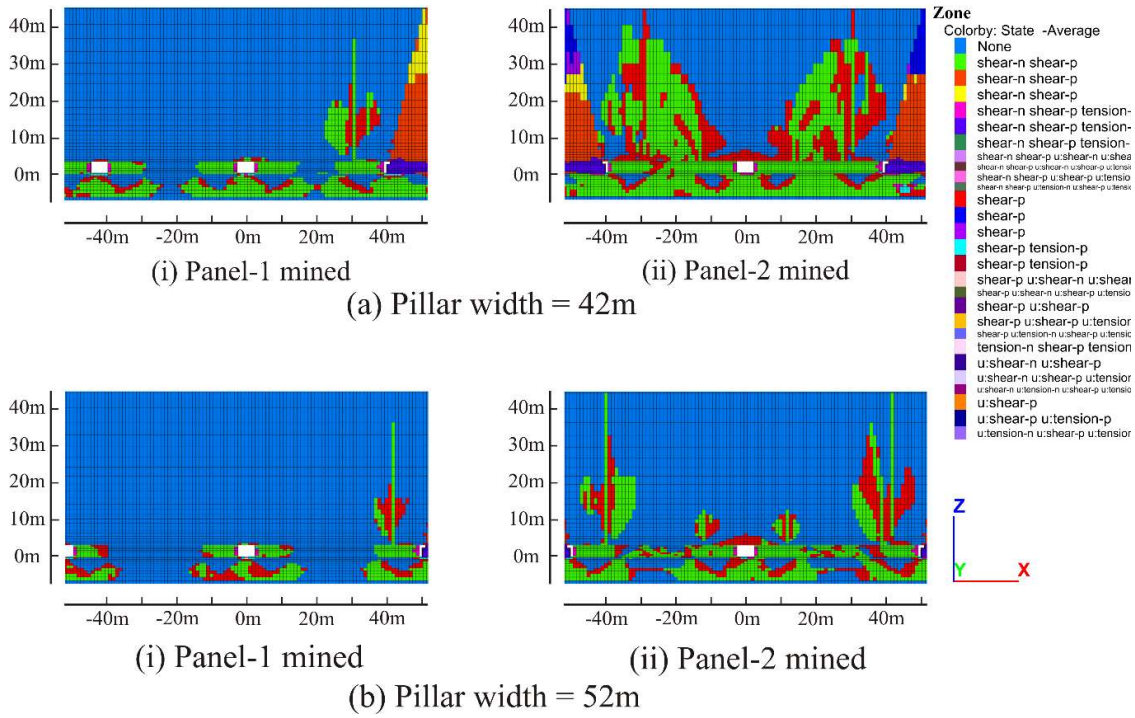

Figure 9.35 Failure state of the pillar system with (i) one-sided goaf and (ii) both-sided goaf for pillar width of (a) 42 and (b) 52 m

After the extraction of the second panel, the entire core of these pillars failed. In the case of 38 m wide pillars, the substantial portion of the immediate roof above the 42 m wide pillars failed, whereas a 45 m high vertical fracture was generated in the immediate roof at a distance of 10 m from the goaf side edges of the pillars of 52 m widths. Most of the floor failed in both cases due to the poor strength of the coal seam 9 m beneath the floor.

Figures 9.36 (a)-(b) show the plot of block contour of vertical stress for the considered pillar widths. It can be seen that the maximum vertical stress was concentrated in the coal at both the

stages of loading in these pillars. Upon the mining of the first panel, the maximum vertical stress was concentrated in the goaf side ribs at 12-14 m depth in Pillar 1 and at 11-13 m depth in Pillar 2 for 42 m width, whereas it was concentrated at 10-12 m depth in Pillar 1 and 10-11 m depth in Pillar 2 in the goaf side ribs of 52 m wide pillar. The peak side abutment stress was located in the goaf side rib of Pillar 1.

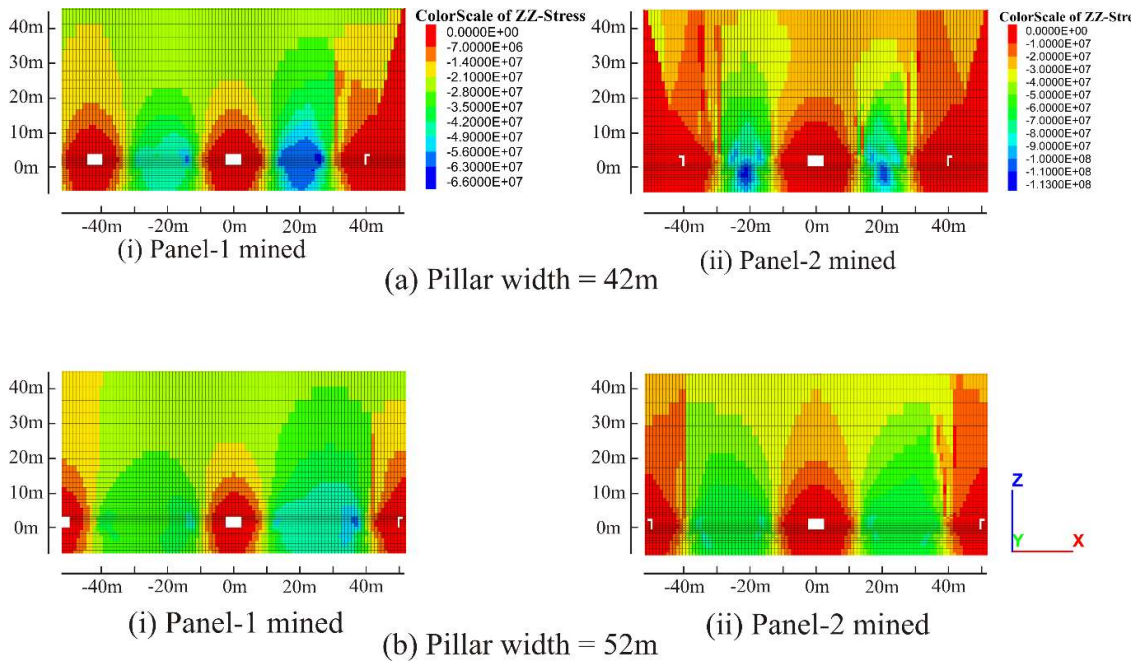

Figure 9.36 Block contour of vertical stress distribution with (i) one-sided goaf and (ii) both-sided goaf for pillar widths of (a) 42 and (c) 52 m

After the extraction of both the panels, the maximum vertical stress in the 42 m wide pillars was observed in the floor below the pillar core due to reduced confinement by the failed roof strata. However, the maximum vertical stress was observed at a distance of 13-15 m from both the edges of the pillars in the case of 52 m wide pillars, as the roof above the core was intact.

Figures 9.37 (a)-(c) show the plot of stress rotation around the excavation at different stages of loading for the optimal pillar width of 42 m. Upon development of the gate roads, the confining stress within 2-3 m at the mid-height of the pillar ribs became negligible (Figure 9.37a). The confinement improved in the inner zone of the pillar as well as towards the roof and floor. The maximum confining stresses were located at the 20-22 m wide core of these pillars.

After the extraction of the first panel, the confining stresses within 3-4 m wide goaf-side rib of pillar 1, 1-2 m tailgate rib of pillar 1 and goaf side rib of pillar 2, and within 1m at the mid-height of the tailgate rib were zero. The confinement increased monotonically towards the core zone of the pillar as well as the roof and the floor. However, the sandstone floor provided substantially greater confinement in the goaf side rib of the pillar in comparison to the immediate roof due to the low abutment angle (Figure 9.37b). The confinement increased gradually in 10-11 m thick ribs of these pillars, and the 16 m core of Pillar 1 and 18 m wide core of Pillar 2 had substantial confinement because of the interface effect and the surrounding failed zones.

When both the panels were mined, the principal stresses in 3-4 m wide ribs of Pillar 1 and Pillar 2 were negligible. The stresses increased towards the core of these pillars. The maximum principal stresses were observed in the sandstone parting below the cores due to lower confinement in the failed pillars and roof owing to the low abutment angle (Figure 9.37c).

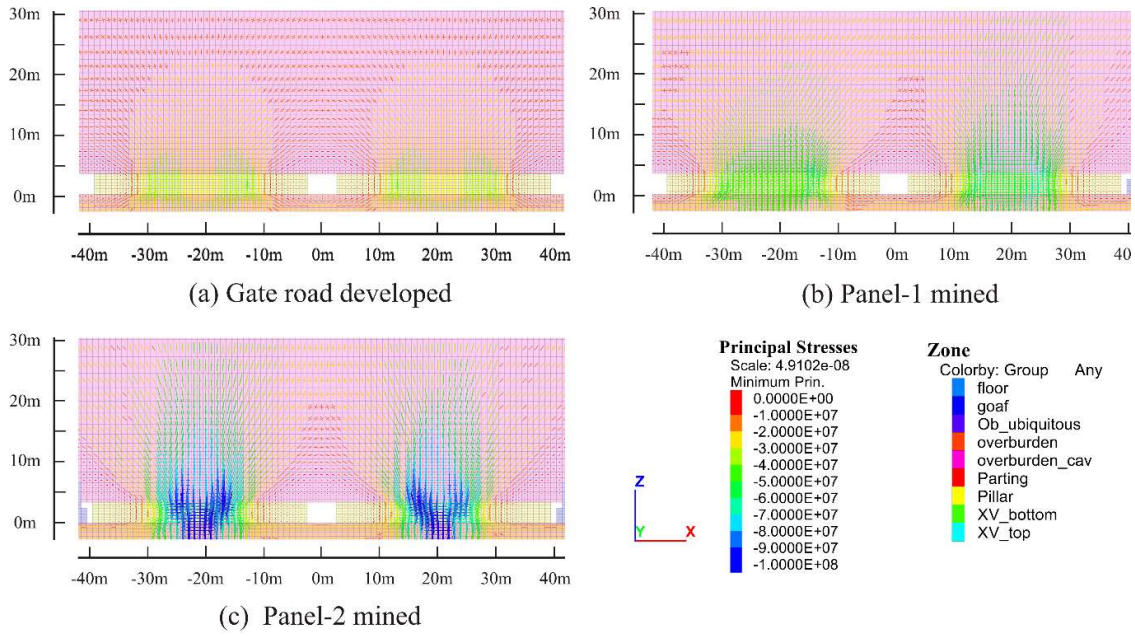

Pillar width = 42m

Figure 9.37 Principal stress tensor plot showing confining stress for the pillar width of 42 m after (a) the development of gate roads, (b) mining of the first panel, and (c) mining of both the adjoining panels

Figure 9.38 shows the bar chart of the tailgate convergence and lateral deformation of the solid coal rib of the second panel and the pillar rib of the gate road entries 1 and 2 upon mining of the first panel. The gate road convergence in entry 1 was 260 mm, while the lateral deformation in ribs of Pillar 1 and 2 was 624 mm and 755 mm, respectively, for the optimum pillar width of 42 m. The convergence in entry 2 was 185 mm, while the rib closure was 532 to 559 mm for this case. With the increase in pillar size to 52m, the convergence reduced to 184 mm in entry 1 and 145 mm in entry 2, while the rib closure was 453 to 515 mm in entry 1 and 427 to 456 mm in entry 2.

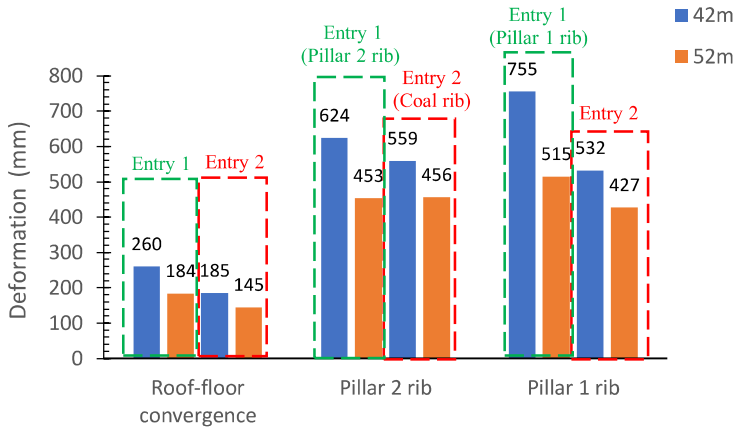

Figure 9.38 Tailgate convergence and lateral deformation in the entry 1 and entry 2 of the second panel for pillar widths of 38, 42, and 52 m upon extraction of the first panel

The high cover depth combined with the poor strength of the coal seam contributed to a closure in the pillar and coal ribs in addition to higher roof-floor convergence in XV Top seam workings. Such large deformations can be controlled using a proper support system to reinforce the ribs and roof, as reported by Zhang et al. (2017b) (Figure 9.39). Zhang et al. (2017b) adopted high-strength bolts/cables with pretension to contain the delamination of the roof layers. Highly pre-tensioned anchor cables were used to clamp the failed roof rock to the stable strata, while pre-tensioned rock bolts improved the integrity of strata in the bolted horizon. The bolts made of high-strength bars had a yield strength of 400 MPa.

Fully grouted rock bolts were used to maintain the integrity of the pillar, as the partially grouted bolts could easily fail under such conditions. Anchor cables and hydraulic supports were used to reinforce the ribs and the roof in front of the approaching face to ensure the integrity of the gate roads during the retreat of the second panel. With the illustrated support pattern, the convergence could be controlled to 516 mm, while the lateral deformation was restricted to 321 to 398 mm at the edge of coal and the pillar ribs in the tailgate.

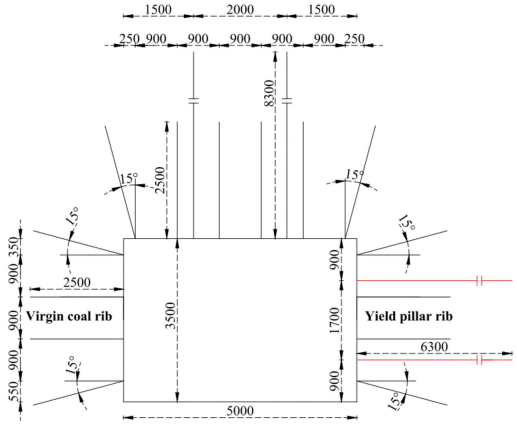

(all dimensions are in mm)

Figure 9.39 Typical support system for containing deformation in longwall gate road (after Zhang et al., 2017b)

9.5 Summary

In this chapter, the numerical modelling approach developed and validated in the previous chapters was utilised to assess the optimum size of the chain pillars for six typical geo-mining conditions belonging to deep longwall workings at Adriyala Longwall Project and Moonidih Colliery. These cases involved chain pillars between panels P1-P2, P2-P3, and P3-P4 in Seam I of Adriyala Longwall Project (ALP) and panels A4-A5 in coal seam XVIII, D12-D13 in coal seam XVI Top, and T3-T4 in coal seam XV Top of Moonidih Colliery. An alternative design with double-row configuration was also worked out for chain pillars between panels T3-T4 for improved ventilation of the working in the Degree III gassy deep seam working at 865m depth, which would also be deep most coal working in India.

The site-specific values of parameters of the 'Double-yield' material model for the 'Caved' zone, the 'Ubiquitous-joint' model for the 'Fractured' zone, and the 'Transversely Isotropic

Elastic' model for the 'Continuous Deformation' zone were estimated using the approach developed in Chapter 6. The abutment angle specific to the geo-mining condition of the workings under study was determined using the statistical model (Equation 7.3) developed in Chapter 7. The optimum pillar size was estimated based on the design criterion developed in Chapter 5. The Machine Learning (ML) model developed in Chapter 8 was also employed to estimate the optimum pillar size to compare its performance with the numerical modelling. The failure behaviour and stress redistribution in these pillars were studied by employing elasto-plastic modelling. The post-peak softening parameters for the pillars were estimated using the statistical model (Equations 4.1-4.4) developed in Section 4.5, Chapter 4.

A parametric modelling study was conducted by varying the width of the chain pillars to obtain their optimum size and comparing its results with the outcome of the Machine Learning (ML) model. The results of both models were in close agreement. The study for Seam I of ALP project at a cover depth varying from 465 – 567m and face length of 250 m showed that the chain pillar size could have been reduced from 63 m to 56 m in panels P2-P3 and 69 m to 60 m in panels P3-P4 that could have helped the mine in reducing the coal loss by 11- 13 % for single-row configuration. The field size pillar of 50m width between panels P1-P2 was found to be optimum. The case study for XVIII seam at the cover depth of 392 m and face length of 95m, XVI seam at cover depth of 568m and face length of 150m, XV seam at the cover depth of 865m and face length of 250m of Moonidih mine showed that the size could have been reduced from the field size of 45 m to 25 m, 50 m to 34 m, and 60 m to 52 m that could have helped in reducing the recovery loss of 13-44% for single-row configuration of the chain pillars in these workings. Table 9.10 summarises the geo-mining and strength parameters associated with the pillar cases along with their optimum pillar width for single-row configuration.

Table 9.10 Geo-mining and strength parameters of the pillars and their optimum size for single-row configuration

Seam, Mine	Panel	Pillar height (m)	Face length (m)	Moduli ratio	Eob	Coal strength (MPa)	Caving height (m)	Depth (m)	Abutment angle (°)	Optimum pillar width (m)
Seam-I, ALP	P1-P2	3.5	250	2.6	5.20	5.65	52.5	465	9.2	51
	P2-P3							519	7.6	56
	P3-P4							567	6.6	60
XVIII, Moonidih	A4-A5	2.55	95	3.11	12.77	2.04	38.25	392	3	25
XVI Top, Moonidih	D12-D13	2.6	150	13.04	12.77	1.08	39	580	4	34
XV Top, Moonidih	T3-T4	3.6	250	49.35	13.40	1.19	54	865	11	52

The mine management faces a significant challenge in meeting the ventilation requirements at the working face with high strata temperature in the deep gassy seam. In such cases, a double row layout becomes inevitable to meet the ventilation requirement. The size of the double row chain pillar for 865m deep XV Top seam working with a face length of 250 m was found to be 42 m.

It can be noted that the cover depth is an essential parameter in determining the size of the pillar. The size of pillars between the panels P2-P3 (56 m) at 465 m depth and P3-P4 (60 m) at 519 m depth increased by 5 m and 9 m, respectively, for an increase of 54 m and 102 m in the cover depth, in comparison to the optimal size pillar between panels P1-P2 (51 m) at 465 m depth. However, the cover depth is not the only parameter to determine the optimal pillar width. For example, the difference between the optimum width of pillar for panels P1-P2 (51 m) at the 465m depth and the single row pillar between panels T3-T4 (52m) at 865 m depth was negligible, although the difference between their cover depth was 400 m. These two cases have approximately the same pillar height, face length, caving height, and abutment angle. However, the moduli ratio for pillar T3-T4 (49.35) was significantly higher as compared to P1-P2, which contributed to its better stability, although the overburden modulus for the latter case was

lower, and the coal strength was higher than in the previous case. The parametric study results also indicated improved FoS of the pillar with the increase in the coal strength and decrease in the overburden modulus.

The optimal size of the pillar between panels D12-D13 (34m) at 580 m depth was 17m less than the pillar between panels P1-P2 (51m), at the cover depth of 465m. The lower face length, pillar height, and caving height (the difference of 100 m, 0.9 m, and 13.5 m, respectively) and 5.02 times higher moduli ratio of pillar D12-D13 in comparison to the P1-P2 pillar contributed to the better FoS, although the former had greater overburden modulus, lower abutment angle and coal strength. The pillars between panels A4-A5 had the smallest optimum size as they had the lowest cover depth, face length, pillar height, and caving height.

The Seam I of Adriyala longwall mine has a weak roof; the rock mass strength of the coal seam (5.65 MPa) and the roof (6.14 MPa) are approximately similar. At the development stage, the failure depth in the pillar ribs varied between 2-3 m in pillars P1-P2, P2-P3 and P3-P4. After the extraction of the first panel, it increased to 3m and 4m in the tailgate side rib of the P1-P2, and P2-P3 and P3-P4 pillars. In the goaf side rib, it extended to 3 m along the bottom end and 6m along the top end of the pillar between panels P1-P2, 4 m along the bottom end and 8m along the top end in pillar P2-P3 and P3-P4. At this stage, the 18-22 m wide immediate roof from the goaf side edge failed in shear. As a result, the peak side abutment stress ranging from 1.78-2.04 times the in-situ vertical stress was concentrated at the tailgate side rib of these pillars. After the extraction of the second panel, the entire immediate roof failed in shear, and a single peak of the side abutment stress was located at the centre of these pillars. However, the failure depth was limited to 6 – 10 m along the bottom and top ends of the pillars between panels P1-P2, 6 - 12 m along the bottom and top ends of the pillars between P2-P3, and 7 – 11 m along the bottom and top ends pillars between P3-P4. The 25 m elastic core was intact in the field size pillar of 50 m width between panels P1-P2. The core of 27 m and 34 m width was

intact of the optimum pillar size of 56 m and field size of 63 m, respectively, in the case of P2-P3, while 37 m and 46 m wide core was intact in the optimum size pillars of 60 m and field size of 69 m width, respectively, in case of P3-P4. The goaf stress recovery of 79, 81, and 85% were realised at the distance of 0.12H from the edge after the extraction of the first panel in P1-P2, P2-P3, and P3-P4 workings, respectively. The stress recovery reached the cover pressure in both the panels after extraction of the second panel.

The XVIII seam at Moonidih Colliery has a moderate strength (2.04 MPa) compared to the immediate roof (8.15 MPa). A 3 m thick rib of the pillar between panels A4-A5 failed at the development stage. After extracting the first panel, the failure depth in the goaf side rib increased to 4 m along the bottom end and 5 – 6 m along the top end of the pillar. The immediate roof was mostly intact. The peak side abutment stress of 2.16 - 2.3 times the in-situ vertical stress was concentrated at the goaf side rib of the pillars. After the extraction of the second panel, the failure depth penetrated to the core of the optimum pillar size of 25 m, and the entire immediate roof failed, while it penetrated to 5-6 m along the bottom end and 9-10 m along the top end in the ribs of the field pillar size of 45 m. The failure of the immediate roof was limited to 20 m from the pillar edges. The 24 m elastic core was intact in the case of the field size pillar. A single peak of side abutment stress was observed at the centre of the optimum size pillar, while a double peak was observed at a distance of about 12 m from the centre in the field size pillar of 45 m width. The goaf stress recovery was 54% of the cover pressure after extraction of the first panel, whereas it increased to 84% and 57% in the first and second panels, respectively, after the extraction of the second panel.

The soft XVI Top seam (in-situ strength of 1 MPa) at Moonidih Colliery is sandwiched between the strong immediate roof and floor (15-24 MPa). The 6 m wide rib of the D12-D13 pillars failed at the development stage. The failure depth increased to 6 and 7 m in the tailgate side rib of the field size pillar of 50 m width and optimal size pillar of 34 m width respectively

between the panels D12-D13. The extent of failure extended to 9 m in the goaf side rib of these pillars, with 1-2 m deeper failure at the top end as compared to the bottom end upon mining the first panel. The peak side abutment stress ranging from 2.5-2.7 times the cover pressure was observed at the goaf side rib of the pillars at this stage. After the extraction of the second panel, while the failure reached the core along the top end of the pillar, the 8 m core did not fail at the top end of the 34 m wide optimal pillar. In the case of the field size pillar of 50 m width, the failure extended to 9-10 m along the bottom end and 14 m along the top end. Hence, a double peak of side abutment stress was observed at the distance of 4 and 14 m from the centre of 34 and 50 m wide pillars. However, the entire immediate roof of the 34 m wide pillar failed in shear, while the immediate roof failed up to 20 m from the edge of the 50 m wide pillar. The stress recovery of 72% of the cover pressure was noted at the distance of 0.06H after the extraction of the first panel, which increased to 88 and 84% for 34 and 50 m wide pillars, respectively, after the extraction of the second panel. The maximum goaf stress in the second panel was 84 and 75% for the 34 and 50 m wide pillars, respectively.

The XV Top seam at Moonidih Colliery is characterised by poor strength (1.19 MPa) and is overlain by a stronger immediate roof (18 MPa). The seam is underlain by a 3 m thick, strong parting of sandstone and a softer coal seam of 3.6 m thickness. A rib failure of 10 m was noted at the development stage of the chain pillar between panels T3-T4 for single-row configuration. The failure depth increased to 11 m and remained constant in the tailgate rib of the optimum size pillar of 52 m and field size pillar of 60 m, respectively. The depth of failure increased to 13 m in the goaf side ribs of these pillars upon extraction of the first panel. A 13 m high vertical fracture line was observed at 8 m depth from the goaf side edge of the pillar. The peak side abutment stress ranging from 2.70-2.83 times the cover pressure was observed at the goaf side rib. After the extraction of the second panel, the entire pillar core of these pillars failed in shear. The complete immediate roof above the 52 m wide pillar failed, while the failure depth in the

immediate roof was limited to 24 m from the edges of the 60 m wide pillar. A single stress peak was observed in the former, while double peaks of stress were observed in the latter, at 14 m from the pillar centre. The goaf stress recovery of 76% of the cover pressure was attained at the distance of 0.1H from the panel edge after the extraction of the first panel, which increased to cover pressure and 88% in the case of 52 and 60 m wide pillars, respectively, after the extraction of the second panel.

In the double row configuration of chain pillars between panels T3-T4, the goaf side pillar (Pillar 1) yielded in shear, whereas the 6-7 m wide core in the optimum pillar width of 38 m was intact in the other pillar (Pillar 2) after the extraction of the first panel. Double stress peaks were observed in these pillars. The peak side abutment stress of 1.8 times the cover pressure was located at a distance of 1m from the centre of Pillar 1. After the extraction of the second panel, a single peak was observed in these pillars. The stress peaks of approximately 3 and 4 times the cover pressure were observed in Pillars 1 and 2, respectively. The entire pillar yielded in shear at this stage. The goaf stress recovery of 75% of the cover pressure was realised at the distance of 0.1H from the panel edge after the extraction of the first panel, while it reached the cover pressure after the extraction of the second panel.

Table 9.11 summarises the convergence in the tailgate and lateral deformation in the pillar and coal ribs of the second panel after extraction of the first panel. The general trend of the convergence and the rib closure showed that their values decreased with the increase in the pillar width. For example, the convergence decreased from 89 to 71 mm, while the lateral displacement at the edge of the coal pillar reduced from 58 to 42 mm and that in the coal rib decreased from 18 to 13mm for the increase in pillar width from 51 to 80 m at the ALP working. The convergence and the rib closure increased with the cover depth, as observed in panels P1-P2, P2-P3, and P3-P4 in the same working.

Table 9.11 Model observed convergence and the rib closure in the tailgate of the second panel after extraction of the first panel

Seam	Pillar	Pillar height (m)	Moduli ratio	Coal strength (MPa)	Depth (m)	Pillar width (m)	Convergence (mm)	Pillar rib closure (mm)	Coal rib closure (mm)
Seam-I, ALP	P1-P2	3.5	5.03	5.65	465	51	89	58	18
						60	83	53	17
						70	76	49	15
						80	71	42	13
	P2-P3				519	56	98	69	25
	P3-P4				567	60	106	78	31
XVIII, Moonidih	A4-A5	2.55	6.3	2.04	392	25	56	51	52
XVI Top, Moonidih	D12-D13	2.6	13.04	1.08	580	3-4	82	144	156
XV Top, Moonidih (Single row)	T3-T4	3.6	49.35	1.19	865	52	185	494	577
XV Top, Moonidih (Double row)	T3-T4 Entry 1					42	260	624	755
	T3-T4 Entry 2						185	559	532

The lateral deformation in the pillar rib was significantly greater than the closure of the coal rib in all the cases of ALP working. It was mainly attributed to the concentration of the peak side abutment stress in the tailgate rib upon failure of the weaker roof above the pillar, which diverted the stresses from over the goaf side rib to the tailgate side rib. The high cover depth combined with the poor strength of the coal seam contributed to the excessive closure of the pillar and coal ribs and convergence in the gate road of the XV Top seam working of Moonidih Colliery. Such large deformations can be controlled using an appropriate system of support to reinforce the ribs and roof of the gate roads, as reported by Zhang et al. (2017b).

Table 9.12 outlines the observed peak side abutment stress after the extraction of the first panel and the recovery of goaf stress when the first and the second panels were mined. The peak side abutment stress increased with the increase in the moduli ratio of the roof-floor to the coal seam. The distance to the maximum pressure (MPD) varies from 0.06-0.12H, which is lesser

than the previously reported values of 0.12-0.6H. The abutment angle in these workings is much less than the values referred by previous researchers (>21°).

Table 9.12 The peak abutment stress and the goaf stress recovery in the workings under study with optimum pillar width

Seam	Pillar	Face length (m)	Moduli ratio	Eob (GPa)	Abutment angle (°)	Peak abutment stress/In-situ stress	Stress recovery (% of cover pressure)			MPD (m)
							P1 mined	P1P2 mined		
							Goaf P1	Goaf P1	Goaf P2	
Seam-I, ALP	P1-P2	250	2.6	5.20	9.2	1.78-2.04	79	100	100	0.12H
	P2-P3				7.6		81	100	100	
	P3-P4				6.6		85	100	100	
XVIII, Moonidih	A4-A5	95	3.11	12.77	3	2.16-2.3	54.3	92	84	0.1H
XVI Top, Moonidih	D12-D13	150	13.04	12.77	4	2.5-2.7	72	88	84	0.06H
XV Top, Moonidih	T3-T4 (Single row)	250	49.35	13.4	11	2.70-2.83	76	100	90	0.1H
XV Top, Moonidih	T3-T4 (Double row)					2.9-3.2	76	100	94	0.1H

The goaf stress recovery in the first panel varied from 54.3-85% of the cover pressure after the extraction of the first panel. The recovered stress increased with the increase in face length. It was minimum for face length of 95 m at 392 m depth and maximum for 250 m face length at 567 m depth. The decrease in the abutment angle and failure of the roof above the goaf side rib of the pillar could be the possible reason for such trends.

Upon the extraction of the second panel, the stress recovery in the first panel was equal to the cover pressure in most cases, except for A4-A5 and D12-D13 at Moonidih Colliery. The stress recovery in the first case was limited to 92% of the cover pressure owing to the smaller face length of 95 m. In the latter case, the strong roof and floor strata led to a small elastic core in the pillar, although the failure reached the core along the roof-pillar contact surface. Hence, the

cover pressure could not be attained. In the second panel, the recovered stress was less than the cover pressure in most cases, except for the ALP working. The lower elastic modulus of overburden and the failure in the weak roof could be the reason for the maximum stress recovery.

The convergence in the tailgate of the second panel after the extraction of the first panel was in good agreement with the field observations. Upon mining the first panel, the decay profile of the side abutment stress followed an exponential relation with the distance from the panel edge, which is in good agreement with the observation of Wilson (1983). The peak side abutment stress varied between 1.68-2.83 times the in-situ stress, which corroborates well with the observations in the Indian geo-mining conditions (Singh and Singh 2009, 2010). The peak stress was located at the tailgate side pillar rib in the ALP workings. The field measurement-based findings of Sinha and Walton (2019a) and the numerical modelling-based findings of Shi et al. (2021) also confirmed the concentration of peak side abutment stress in the tailgate rib of the pillar under the relatively weaker immediate roof.

Further, the optimum size pillar in all the cases under study had a single peak, whereas the oversized experimental and field pillars had double peaks after the extraction of both the panels. This observation is in line with the work of Yu et al. (2016), who opined that the pillar size equal to the distance between the two peaks could be reduced without compromising the performance of the pillar. The convergence and the closure of the ribs in the gate road decreased with the increase in pillar width but increased with cover depth, which is in good agreement with the field observation of Whittaker and Singh (1979).